Ether and ester formation from peroxy radical recombination: A qualitative reaction channel analysis

Lauri Franzon[a], Marie Camredon[b], Richard Valorso[b], Bernard Aumont[b], and Theo Kurtén[a]

[a]Department of Chemistry, University of Helsinki, P.O. Box 55 (A.I. Virtasen aukio 1), 00014 Helsinki, Finland
[b]Univ Paris Est Creteil and Université Paris Cité, CNRS, LISA, F-94010 Créteil, France

Correspondence: Lauri Franzon (lauri.franzon@helsinki.fi) and Theo Kurtén (theo.kurten@helsinki.fi)

Abstract. The least volatile organic compounds participating in atmospheric new-particle formation are very likely accretion products from self- and cross-reactions of peroxy radicals (RO_2). It has long been assumed that the only possible accretion product channel in this reaction is that forming a peroxide ($RO_2 + RO_2 \longrightarrow ROOR + O_2$), but it has recently been discovered that a rapid alkoxy radical (RO) decomposition may precede the accretion step of the mechanism, forming slightly fragmented but more stable ether (ROR) or ester ($RC'(O)OR$) accretion products. In this work, the atmospheric implications of this new reaction channel have been explored further using a modified version of the GECKO-A software to generate a large amount of representative $RO_2 + RO_2$ reactive pairs formed from the oxidation of typical primary hydrocarbons, and applying Structure-activity relationships ~~(SAR)~~ to predict the potential accretion products. This data is analysed in terms of formation of low-volatility products, and new discoveries are presented on what kind of RO_2 are especially efficient (and which are surprisingly inefficient) at forming accretion products. These findings are discussed in terms of atmospheric relevance of these new $RO_2 + RO_2$ reaction channels. As the generation of this data rests on several simplifications and assumptions, many open questions worthy of later studies are also raised.

1 Introduction

1.1 Atmospheric Background

The formation and growth of secondary organic aerosol particles (SOA) in pristine environments is dependent on gas-phase formation of low volatility organic molecules, but the exact formation pathways of such organics is only partially known (Kanakidou et al., 2005). The self- and cross reactions of peroxy radicals (RO_2) are assumed to be important sources of such low-volatility molecules, (Berndt et al., 2015) as this is one of the rare cases of gas-phase atmospheric reactions where *accretion products*, products with a larger carbon count than the reactant radicals, can form. The previously known accretion product forming pathway of these recombination reactions is a peroxide connecting the carbon skeletons of the reactant RO_2 in the reaction $RO_2 + RO_2 \longrightarrow ROOR + O_2$. This is however not the only possible product of the reaction, and we will therefore briefly review the history of studies on the reaction. The mechanism of RO_2 recombination has been known to go through an unstable tetroxide intermediate since the proposed 'Russell mechanism' for its decomposition (Russell, 1957). However, the

currently accepted mechanism for the reaction was presented by Ingold (Ingold, 1969), in which the tetroxide ejects an O_2 molecule, leaving behind a triplet state bimolecular complex of two alkoxy radicals, ^{3}(RO…OR):

$$\begin{aligned} &\mathrm{RO_2 + RO_2 \longleftrightarrow RO_4R} \\ \longrightarrow\ &^1(\mathrm{RO\ldots O_2\ldots OR}) \longrightarrow\ ^3(\mathrm{RO\ldots OR}) + {}^3\mathrm{O_2} \end{aligned} \tag{R1}$$

Recent theoretical studies indicate that in the case of CH_3O_2 + CH_3O_2 recombination the ejection of one CH_3O radical from the ($CH_3O\ldots O_2\ldots OCH_3$) complex is thermodynamically (but not necessarily kinetically) favourable to that of O_2 (Salo et al., 2024). Recent experimental studies also suggest a novel in-complex ($RO\ldots O_2$) $\longrightarrow R_{\text{-H}}{=}O + HO_2$ reaction channel from the self-reaction of the $HOC_2H_4O_2$ radical (Murphy et al., 2023). Here we will however operate from the assumption that these reactions are only possible for very weakly bound systems, and that channel R1 is exclusively the fate of generic $RO_2 + RO_2$ reactions. In the mechanism proposed by Ingold (1969), the ^{3}(RO…OR) complex has three further reaction channels, a dissociation pathway (Reaction R2) into two free alkoxy radicals (RO), an intermolecular H-shift (Reaction R3) forming an alcohol and a carbonyl, and an Intersystem Crossing (ISC) into the singlet state followed by barrierless recombination into a peroxide accretion product (Reaction R4, ROOR). The branching ratios for these three pathways have been studied both experimentally (Orlando and Tyndall, 2012) and computationally (Hasan, 2023). In our previous work, (Peräkylä et al., 2023) we found an unexpected fourth reaction channel for an α-pinene derived ^{3}($C_{10}H_{15}O_2O\ldots OC_{10}H_{15}O_2$) complex, in which one of the alkoxy radicals undergoes a rapid β-scission reaction, thereby producing a $C_{19}H_{28}O_5$ ester accretion product. Assuming these kinds of reactions are possible for other systems as well, we may update the full mechanism of peroxy radical recombination to include the following four pathways:

$$^3(\mathrm{RO\ldots OR}) \xrightarrow{\text{Dissoc}} \quad \mathrm{RO + RO} \tag{R2}$$

$$\xrightarrow{\text{H-Shift}} \quad \mathrm{R_{-H}{=}O + ROH} \tag{R3}$$

$$\xrightarrow{\text{ISC}} \quad \mathrm{ROOR} \tag{R4}$$

$$\xrightarrow{\text{RO Dec}} \quad \mathrm{ROR'\ (+P)} \tag{R5}$$

where R′ denotes that the original organic R group may be fragmented, in which case P is the second fragmentation product (CH_2O is the case of the previously mentioned $C_{19}H_{28}O_5$ ester product). The computational results provided by Peräkylä et al. (2023) suggested that the occurrence of channel R5 depends on the unimolecular decomposition rate of the RO outspeeding reaction channels R2, R3 and R4, on which we already have produced a body of computational work. The rate of the dissociation channel is primarily predicted by the binding energy of the ^{3}(RO…OR) complex, ranging from $2\cdot10^1$ s^{-1} to $8\cdot10^{10}$ s^{-1}. (Franzon, 2023) Dissociation is therefore likely to be uncompetitive for larger, more functionalized, and thus more strongly binding pairs of RO. An equally unambiguous trend for the H-shift rate has proved difficult to determine (Hasan et al., 2023), but the computed H-shift rates show a weak negative correlation with the binding energy, suggesting that this pathway is also less competitive for larger and more functionalized radicals. These H-shift rates are rarely above 10^9 s^{-1}. It is also notable that

only primary and secondary RO can act as H donors, meaning that this channel does not exist at all if both of the reacting RO_2 are either acyl peroxy radicals ($RC(O)O_2$) or tertiary RO_2. The ISC rate seems to be systematically on the order of 10^9 s^{-1}, with the ~~^{3}(MetO…OMet)~~ $^3(CH_3O\ldots OCH_3)$ complex and some stereoisomers of ONO_2-substituted RO acting as outliers (Hasan, 2023). In summary, if reaction channels of type R5 are of any significance, they must outspeed the ISC rate if the ^{3}(RO…OR) is strongly binding, as well as the dissociation and bimolecular H-shift rates if the complex is weakly binding. Based on the information above, it seems that the RO decay rate must be close to 10^8 s^{-1} to be of any importance, and preferably above 10^9 s^{-1} to be a main channel.

The in-complex RO decomposition we observed (Peräkylä et al., 2023) was a β-scission reaction forming an acyl-centered radical combining with the other RO to form an ester. Similar reactions forming alkyl radicals as decomposition products will presumably result in ether accretion products. Decay rates of RO radicals inside complexes are currently unknown, but as a first approximation we may estimate them using the corresponding reaction rates of free RO. This is convenient, as the atmospheric reactions of alkoxy radicals have already been studied widely. The Structure-Activity Relationship (SAR) by ~~Vereecken and Peeters (2009)~~ Vereecken and Peeters (2009); Novelli et al. (2021) for β-scission reactions of free RO suggests that there are multiple chemical structures that reach the approximate threshold of 10^8 s^{-1}, suggesting that this channel may be quite common. We also ought to entertain the possibility that β-scission reactions are not the only kind of unimolecular RO reaction which may occur in-complex. A review on the atmospheric chemistry of alkoxy radicals by Orlando et al. (2003) discussed three additional reaction classes for (non-halogenated) RO: unimolecular H-shifts, ester rearrangement and O_2 addition. Upon closer examination however, only the unimolecular H-shift pathway is reportedly fast enough to cross our importance threshold of 10^8 s^{-1} in some known cases, as the ester rearrangement and O_2 addition pathways are both limited to (pseudo-unimolecular in the latter case) rates of around 10^5 s^{-1}. To avoid confusion between H-shift reactions of type R3 and type R5, we shall be referring to the former as *bimolecular* H-shifts and the latter as *unimolecular* H-shifts.

In this work, we aim to explore the wider atmospheric significance of channel R5 using a $RO_2 + RO_2$ accretion product generator code based on the GECKO-A (Generator for Explicit Chemistry and Kinetics of Organics in the Atmosphere (Aumont et al., 2005)) software, which we call GECKO-AP (... of Organic Accretion Products). GECKO-AP makes use of all the RO_2 and RO chemistry already included in GECKO-A, combined with simple parametrizations of the knowledge we currently have of the competing reaction channels to generate datasets of all the possible peroxide, ether, and ester accretion products derived from a GECKO-A-generated set of RO_2. These datasets of accretion products are then analysed in order to learn which of these reactions are most important, especially when it comes to the formation of low-volatility products. The purpose of this article is not to determine accurate branching ratios for these channels, as this most likely requires both characterization of further ester or ether product from experiments, as well as extensive computations benchmarked against such experiments. Instead, the purpose of this work is to inform future efforts on where to start looking, and to assess general qualitative features of accretion products formed by the recently discovered pathways.

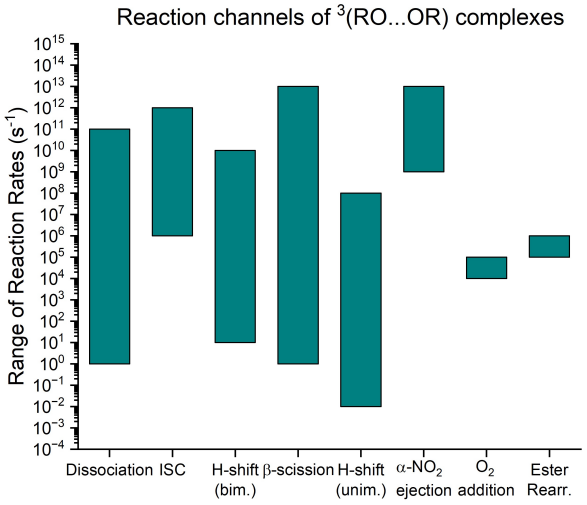

Figure 1. A visualisation of the range of rates of the three known reaction channels of ^{3}(RO…OR) complexes compared to the unimolecular reaction rates of free RO radicals considered in this work. The range of dissociation rates are from Franzon (2023), the ISC and bimolecular H-shifts from Hasan (2023), the β-scission and unimolecular H-shift rates from Vereecken and Peeters (2009) and Vereecken and Peeters (2010), and the O_2 addition and α-ester rearrangement from Orlando et al. (2003). The α-NO_2 ejection is discussed in Sect. 2.1.4.

1.2 GECKO-A

In order to place the importance of reaction R5 in a wider atmospheric context, a large selection of atmospherically relevant peroxy radicals must be screened to determine the cases where these in-complex decomposition reactions are competitive. For this purpose, GECKO-A was used to generate large numbers of atmospherically relevant RO_2. As GECKO-A only generates the products from channels R2 and R3 for RO_2 recombination reactions according to the parametrization presented in Jenkin et al. (2019), a new code was written to generate all the possible accretion products (both channels R4 and R5) from each individual pair of RO_2. The structure of the code is described in detail in Sect. 2.1. Using this code, three large accretion product datasets from representative precursor molecules were produced, which are presented in Sect. 2.2 and analysed in detail in Sect. 3 to determine two things: What the existence of reaction channel R5 implies for the formation of low-volatility products from RO_2 recombination, and which aspects of this channel are worth studying in more detail.

The GECKO-A tool generates explicit atmospheric chemical mechanisms from a list of organic precursors provided as input. The chemistry included in the version of GECKO-A used to generate the data was VOC oxidation by OH (Jenkin et al., 2018a, b), alkene oxidation by O_3 (Jenkin et al., 2020), VOC oxidation by NO_3 (Kerdouci et al., 2014), photolysis for some select chromophores Aumont et al. (2005), thermal decomposition of peroxy acyl nitrates ($-$C(O)OONO$_2$) (Jenkin et al., 2019), RO decomposition (Vereecken and Peeters, 2009), (mostly bimolecular) reactions of RO_2 (Jenkin et al., 2019) and stabilized

Criegee Intermediate chemistry (Newland et al., 2022). All generated molecules are grouped by *generation* based on the minimum number of stable closed-shell species that are produced in the formation of that molecule. For example, CH_2OHCH_2OOH and $CH_2(ONO_2)CH_2OOH$ are 1st generation products of ethene. The molecules produced from the oxidation of these (including the radicals) are 2nd generation products, and so on. The GECKO-A molecule generator creates all the oxidation pathways up to a specified generation n and above a specified critical saturation vapour pressure p_c (Aumont et al., 2005). In this study, the generated chemical mechanisms were used to provide lists of peroxy radicals expected to be representative of typical atmospheric RO_2, in their structure, but also in their probability to be formed. ~~A~~ GECKO-A also calculates a theoretical maximum yield of formation ~~,~~ parameter y, ~~was therefore calculated from the chemical mechanisms for each RO_2. For competitive chemical pathways, the formation yield depends of the concentration of~~ which is used to filter out minor reaction channels is the mechanism generation. As the mechanism generator code makes minimal assumptions on environmental conditions such as relative humidity, and bimolecular reactant (such as OH, O_3, NO_3, HO_2, NO, NO_2 and RO_2~~lumped into reaction rate classes) , which change with environmental chemical conditions. A maximum yield of 100 % was therefore considered for each of these competing pathways.~~) concentrations, this parameter does not account for competition between different bimolecular reactions. The maximum yield is therefore 'theoretical' in the sense that the y value of (for example) Isoprene + NO_3 products correspond to real yields in conditions where Isoprene oxidation is completely dominated by NO_3. This means the y values have the disadvantage of occasionally over-representing products with high yields from slow reactions, but from the perspective of our qualitative $RO_2 + RO_2$ reaction channel analysis, the environmental independence is an advantage, as it allows us to treat all hypothetically possible atmospheric $RO_2 + RO_2$ reactions uniformly without the loss of generality. The y values of the RO_2 generated by GECKO-A were thus used as a filter with which to select $RO_2 + RO_2$ pairs for further treatment. A comparison of theoretical maximum yields with simulated formation rates and concentrations is performed in Section S8 in the Supplement.

2 Methods

2.1 Generation of Accretion Product datasets

As the scope of this work is limited to exploring the potential accretion products, the GECKO-AP code was built to simply generate a list of $RO_2 + RO_2$ accretion products from a list of RO_2 generated in the GECKO-A mechanism. In this section, the process of creating accretion products datasets from an RO_2 list is described in detail. As the potential number of pairings increases combinatorically with the length of the RO_2 list ($N + \frac{N!}{2!(N-2)!} = \frac{N^2}{2} + \frac{N}{2}$), care was taken to efficiently filter out all of the least important radicals (Sect. 2.1.1), least probable $RO_2 + RO_2$ pairs (Sect. 2.1.2 and 2.1.3), and least competitive product channels (Sect. 2.1.5) in the code.

2.1.1 Filtering of individual RO_2

The list of RO_2 radicals generated in a GECKO-A mechanism was used as input for the GECKO-AP code, with some filtering done to reduce the number of products. First, a yield cutoff y_c was chosen such that all RO_2 with theoretical maximum yield

$y < y_c$ were filtered out. Second, CH_3O_2 was systematically left out as a rule from these lists, as all of our previously studied $^3(CH_3O\ldots OR)$ systems have had rapid dissociation (Franzon, 2023) and bimolecular H-shift (Hasan et al., 2023) rates. We thus suspect that CH_3O_2 + RO_2 reactions are not a significant source of accretion products in the atmosphere, and most certainly not a source of large, low-volatility accretion products. Third, $RC(O)O_2$s with hydroperoxide (OOH) substituents were also excluded, as the rapid H-scrambling reaction into a peracid-substituted alkyl peroxy radicals is expected to be effectively irreversible. (Knap and Jørgensen, 2017) As GECKO-A currently lacks RO_2 H-shift and H-scrambling reactions, a simple exclusion of these radicals from partaking in RO_2 + RO_2 was seen as a suitable correction.

2.1.2 Filtering of RO_2 pairs by probability

Another method of filtering out the least important data is to only treat the RO_2+RO_2 pairs above a certain probability threshold, which in the GECKO-AP code is formulated in terms of $RO_2 + RO_2$ reaction kinetics. The formation rate of a $^3(RO\ldots OR)$ complex is:

$$\frac{\mathrm{d}[(\alpha\ldots\beta)]}{\mathrm{d}t} = k_{\mathrm{RO_2RO_2}}[\alpha][\beta] \tag{1}$$

Here $[\alpha]$ and $[\beta]$ are the concentrations of the two reacting peroxy radicals, and $k_{\mathrm{RO_2RO_2}}$ is the recombination rate coefficient. Since the best estimation we have of individual RO_2 concentrations in the GECKO-A mechanism generator is the theoretical maximum yield y, we will estimate an equivalent *recombination yield* using these:

$$y_{\alpha\beta\mathrm{RO_2RO_2},\alpha\beta} = k_{rel} y_\alpha y_\beta \tag{2}$$

where y_α and y_β are the theoretical maximum yields of the RO_2 α and β. Since a yield must be between 0 and 1 by definition, the rate coefficient k_{rel} must also be expressed relative to some maximum~~. We must also consider the fact that $RO_2 + RO_2$ yields are also impacted by the other reaction rates of the radicals. We will start from a simplified equation where unimolecular RO_2 reaction are neglected, and where the peroxy radicals form an uniform 'pool' with concentration $[RO_2]$. In this case the yield of $RO_2 + RO_2$ is:~~

$$y_{\mathrm{RO_2RO_2}} = \frac{k_{\mathrm{RO_2RO_2}}[\mathrm{RO_2}]^2}{k_{\mathrm{RO_2RO_2}}[\mathrm{RO_2}]^2 + \sum_i^5 k_i[\mathrm{Ox}]_\mathrm{i}[\mathrm{RO_2}]}$$

~~Where the summation is over the other five bimolecular reactions: $RO_2 + NO$, $RO_2 + NO_2$, $RO_2 + NO_3$, $RO_2 + OH$ and $RO_2 + HO_2$. Oxis the concentration for one of these five reactants. The $RO_2 + RO_2$ reaction being a minor RO_2 loss in most atmospheric conditions, it is notable that the relationship between $y_{\mathrm{RO_2RO_2}}$ and $RO_2$is linear at low concentrations: $y_{\mathrm{RO_2RO_2}} \approx \frac{k_{\mathrm{RO_2RO_2}}}{\sum_i^5 k_i[\mathrm{Ox}]_i}[\mathrm{RO_2}]$. Next, we will derive the ratio of $y_{\mathrm{RO_2RO_2}}$ between two RO_2 with different rate coefficients but identical concentrations:~~

$$\frac{y_{\mathrm{RO_2RO_2},\alpha}}{y_{\mathrm{RO_2RO_2},\beta}} = \frac{k_{\mathrm{RO_2RO_2},\alpha}}{k_{\mathrm{RO_2RO_2},\beta}} \times \frac{k_{\mathrm{RO_2RO_2},\beta}[\mathrm{RO_2}]^2 + \sum_i^5 k_{i,\beta}[\mathrm{Ox}]_i[\mathrm{RO_2}]}{k_{\mathrm{RO_2RO_2},\alpha}[\mathrm{RO_2}]^2 + \sum_i^5 k_{i,\alpha}[\mathrm{Ox}]_i[\mathrm{RO_2}]}$$

$$\approx \frac{k_{\mathrm{RO_2RO_2},\alpha}}{k_{\mathrm{RO_2RO_2},\beta}} \times \frac{\sum_i^5 k_{i,\beta}[\mathrm{Ox}]_i}{\sum_i^5 k_{i,\alpha}[\mathrm{Ox}]_i}$$

~~As we see, this ratio is a constant at the low RO_2limit. Next, we need to consider whether the $\frac{\sum_i^5 k_{i,\beta}[\mathrm{Ox}]_i}{\sum_i^5 k_{i,\alpha}[\mathrm{Ox}]_i}$ may play a role in shifting specific recombination yields up or down. In their review and parametrization of RO_2 reaction rates and branching ratios, Jenkin et al. (2019) recommend using a single generic reaction rate for all $RO_2 + OH$ reactions. For the three $RO_2 + NO_x$ reactions, one generic rate is recommended for alkyl RO_2 and a second for acyl RO_2. The same is suggested for the $RO_2 + HO_2$ reaction, both with an additional RO_2 size-dependent factor $(1 - e^{-0.23 n_{HA}})$, where n_{HA} is the number of non-H atoms in the R functionality. Differences caused by this factor are all within a factor of 2 for $n_{HA} > 3$ and within a factor of 1.1 for $n_{HA} > 10$, so likely this will only cause significant differences in lifetimes for small RO_2 in HO_2-dominated conditions. In summary, then, the relative impact of the $\frac{\sum_i^5 k_{i,\beta}[\mathrm{Ox}]_i}{\sum_i^5 k_{i,\alpha}[\mathrm{Ox}]_i}$ 'rate-to-yield'-factor on RO_2 recombination yields only needs to be considered for $RC(O)O_2$. In theory the value of this factor depends on the concentrations of the bimolecular reactants NO, NO_2, NO_3, OH and HO_2, as well as on the $RC(O)O_2$ size. However, for code optimization purposes we would prefer to use a single value that does not need to be calculated separately, and that neither overrepresents high-NO_x or low-NO_x conditions. For this reason, the following arbitrary intermediate level values were chosen for each reactant: $[\mathrm{NO}] = [\mathrm{NO_2}] = 2 \cdot 10^9$ molecule cm^{-3} (100 ppt), $[\mathrm{NO_3}] = 10^8$ molecule cm^{-3}, $[\mathrm{OH}] = 10^6$ molecule cm^{-3}, $[\mathrm{HO_2}] = 10^7$ molecule cm~~

~~With these concentrations the value of the rate-to-yield factor for $RC(O)O_2$ is 0.56.~~

~~For~~ for which we use the $RO_2 + RO_2$ rate coefficient for the GECKO-A RO_2 class 8 (See Table 3): $k_{rel} = \frac{k_{\mathrm{RO_2RO_2}}}{5.3 \cdot 10^{-12}\ \mathrm{cm^3\ molecule^{-1}\ s^{-1}}}$.

The $RO_2 + RO_2$ ~~cross-reactions, the reaction rates are~~ rate coefficient is determined using a slight simplification of the scheme described in the Supplement of Jenkin et al. (2019), where the individually calculated self-reaction rate coefficient is replaced by one of the nine GECKO-A RO_2 class rates (Table 1). This way k_{rel} can be efficiently calculated for large numbers of RO_2 pairs without using up memory for self-reaction rates. As suggested by Jenkin et al. (2019), cross reactions between $RC(O)O_2$ and other RO_2 are always treated as collision-limited, whereas other rates are determined using a geometric mean of the two self-reaction rates, with an additional factor of 2 for reactions between tertiary and primary or secondary RO_2 ($f_{\mathrm{t^+ps}}$).

$$k_{\mathrm{RO_2RO_2},\alpha+9} = 1.1 \cdot 10^{-11}\ \mathrm{cm^3\ molecule^{-1}\ s^{-1}} \tag{3a}$$

$$k_{\mathrm{RO_2RO_2},\alpha+\beta} = 2 f_{\mathrm{t^+ps}} \sqrt{k_{\mathrm{RO_2RO_2},\alpha} \cdot k_{\mathrm{RO_2RO_2},\beta}} \tag{3b}$$

~~Furthermore,~~ For reactions between $RC(O)O_2$ and other radicals, two additional correction factors are used to scale down the yields. Firstly, as GECKO-A lacks unimolecular H-shift (autoxidation) reactions for peroxy radicals, the recombination yields of $RC(O)O_2$ other than ~~MetC(O)O$_2$~~ $CH_3C(O)O_2$ were scaled down based on an uniform autoxidation sink of 1 s^{-1}. ~~The motivation for this choice is given in Sect. S2 of the Supplement. With both of these corrections applied to the RC(O)O$_2$~~

~~recombination rates , in practice the maximum recombination rate which we use as reference for k_{ref} in Eq 2 is the GECKO-A class rate 8 (Table 1)~~Secondly, we must also consider that bimolecular reactions between $RC(O)O_2$ and common atmospheric inorganic radicals (OH, HO_2, NO_x) are generally faster than the corresponding reactions for alkyl RO_2, which means that the relationship between the faster recombination rates of $RC(O)O_2$ and the resulting recombination yields is not directly comparable. Thus, we apply a 'rate-to-yield factor' of 0.56 to $RO_2 + RO_2$ reactions involving acyl peroxy radicals based on a quick derivation of the relationship between the rates and the yield. More details are given in Sect. S2 of the Supplement. To summarize, we may rewrite Eq 2 in the form used in the GECKO-AP code:

$$y_{\alpha\beta \mathrm{RO_2RO_2},\alpha\beta} = f_9 \frac{k_{\mathrm{RO_2RO_2},\alpha+\beta}}{k_8} y_\alpha y_\beta \tag{4}$$

where k_8 is the $RO_2 + RO_2$ rate coefficient for rate class 8, and f_9 is the correction applied to $RO_2 + RC(O)O_2$ reactions, which if 1 if neither α or β are $RC(O)O_2$, 0.56 if ~~one either is MetC(O)O$_2$~~either is $CH_3C(O)O_2$, and 0.035 if either is some other $RC(O)O_2$ (see Supplement). To filter out less probable RO_2 pairs, a cutoff yield y_c is defined below which the $RO_2 + RO_2$ pair is not considered. The same value is used to filter out individual RO_2, as $y_\alpha < y_c$ directly implies $y_{\alpha\beta} < y_c$.

Class	Description	Rate ($\frac{\mathrm{cm}^3}{\mathrm{molecule\ s}}$)
1	unsubstituted tert-RO_2	$2.1 \cdot 10^{-17}$
2	i-$C_3H_7O_2$	$1.0 \cdot 10^{-15}$
3	tert-RO_2 with α- or β- O or N	$7.9 \cdot 10^{-15}$
4	$C_2H_5O_2$; unsubstituted sec-RO_2;	$6.9 \cdot 10^{-14}$
5	tert-RO_2 with α- or β- O or N and allylic or β-aryl group	$1.0 \cdot 10^{-13}$
6	CH_3O_2	$3.5 \cdot 10^{-13}$
7	unsubstituted prim-RO_2; sec-RO_2 with α- or β- O or N	$1.1 \cdot 10^{-12}$
8	prim-RO_2 with α- or β- O or N; sec-RO_2 with α- or β- O or N and allylic or β-aryl group	$5.3 \cdot 10^{-12}$
9	Acyl peroxy radicals	$1.4 \cdot 10^{-11}$

Table 1. The nine $RO_2 + RO_2$ rate classes used in GECKO-A, adapted from Jenkin et al. (2019).

2.1.3 Filtering of RO_2 pairs with rapid dissociation

As we are primarily interested in the accretion product forming channels R4 and R5, it also makes sense to filter out RO_2 pairs for which the branching ratios of channels R2 and R3 can be presumed to be high. As experimental data on these branching ratios is still relatively scarce, we are not able to create reliable SAR calculators for the rates of channels R2 and

R3, let alone branching ratios. However, the results from our previous computational studies (Franzon, 2023; Hasan, 2023) indicate that both of these rates are negatively correlated with the binding energy of the $^3(\mathrm{RO}\dots\mathrm{OR})$ complex. It has been suggested elsewhere (Peräkylä et al., 2023) that the ability of the RO to form intermolecular H-bonds is key to suppressing these two channels and especially channel R2. ~~These H-bonds are counted for each RO_2 pair in the GECKO-AP code~~ , and this might offer us a viable approach to filter out ~~the pairs that form weakly bonded complexes~~ RO_2 pairs with weakly-bound $^3(\mathrm{RO}\cdot\cdot\mathrm{OR})$ complexes using only the information available to the mechanism generator. For this purpose, **-OH, -OOH, -C(O)OH and -C(O)OOH** were treated as H-bond donating groups, whereas **-CHO, -C=O-, -C(O)OH, -C(O)OOH, -NO_2, -ONO_2, -$OONO_2$, -C(O)$OONO_2$** as well as the radical oxygen were treated as H-bond accepting groups. In addition, every C-H bond (aliphatic or aromatic) was treated as a partial H-bond donor, as these may stabilize larger $^3(\mathrm{RO}\dots\mathrm{OR})$ complexes in the presence of H-bond acceptors, as noted in the Supplementary of Peräkylä et al. (2023). Using these parameters, an *effective H-bond number* (HBN) was calculated for each pair of alkoxy radicals:

$$HBN_{\alpha,\beta} = n_{\mathrm{D},\alpha} \cdot n_{\mathrm{A},\beta} + n_{\mathrm{D},\beta} \cdot n_{\mathrm{A},\alpha} \tag{5}$$

Where D and A respectively refer to donor and acceptor, and α and β refer to the two ~~complexes RO . The value of this parameter was benchmarked against the binding energies of~~ RO in the complex. Regarding the specific form of the equation, we emphasize that the purpose of the equation is to mimic the observed trends in $^3(\mathrm{RO}\cdot\cdot\mathrm{OR})$ binding energies, which do not exclusively depend on the ability to form H-bonds, but also on dipole-dipole bonds, dispersion interactions, and on Pauli repulsion of the two radical oxygens. Out of these secondary interactions, the dipole-dipole bonding largely depends on the presence of the same functional groups as the H-bonding interactions, at least in the context of gas-phase organic chemistry. This means that we were able to get a good agreement (a correlation coefficient of ≈ 0.92) between the $HBN_{\alpha,\beta}$ value and the binding energies of ^{3}(RO…OR) complexes presented by Hasan (2023) ~~and the~~ by adjusting the 'partial H-bond donor' value assigned to each C-H bond. The optimal value chosen used in the code was 0.04. Based on the dissociation rates calculated using these binding energies (Franzon, 2023). ~~Based on these results~~, a HBN cutoff of 1.75 was chosen, below which accretion products are not generated for that specific RO_2 pair. ~~Each C-H bond was treated as 1/25th of a H-bond donor when calculating this value.~~ The full analysis of how this cutoff was chosen is described in Sect. S1 of the Supplement.

2.1.4 In-complex RO reactions

For all RO_2 in the input list, a systematic search of decomposition reactions is performed for the corresponding RO. The approach for finding the reactions is done very similarly as in the ordinary GECKO-A code (Aumont et al., 2005). As discussed in the introduction, the following three reaction classes were judged to potentially be competitive in-complex:

1. β-scission, which turns the alkoxy moiety into a carbonyl and the site of the broken bond into an alkyl radical. The search is performed similarly as in the base GECKO-A code for free alkoxy radicals, relying mainly on Vereecken's & Peeters's Structure-Activity Relationship (SAR) (Vereecken and Peeters, 2009; Novelli et al., 2021).

2. A unimolecular H-shift to the alkoxy oxygen resulting in the formation of an alkyl radical with one additional OH substituent. This relies mainly on Vereecken's and Peeters's SAR. (Vereecken and Peeters, 2010)

3. α-NO_2 ejection, resulting in a carbonyl and a NO_2 radical. This reaction is set to an arbitrarily high ($k_{\alpha-\mathrm{NO_2}} = 10^{12}\ \mathrm{s^{-1}}$) rate in GECKO-A to conveniently get rid of these compounds. As this reaction happens to have interesting implications for accretion product formation (See Sect. 3.3), computational rate coefficients were calculated for a set of small representative compounds using the ORCA software. (Neese, 2022) According to these calculations the reaction will typically have rates closer to the $[10^9\ \mathrm{s^{-1}}, 10^{10}\ \mathrm{s^{-1}}]$ range, which is still highly competitive in-complex. Computational details are found in Sect. S3 of the Supplement.

The rates of all reactions for each individual RO are compared, and all channels found to be competitive enough to at least be minor products (using a branching ratio cutoff of 0.05) next to an assumed universal ISC rate of $10^9\ \mathrm{s^{-1}}$ are considered for in-complex reaction branching ratio calculations.

For every reaction, the stability of the radical product is checked by running through a list of barrierless decomposition reactions. This was done utilizing a version of the code described in Sect. 3.1 of Aumont et al. (2005), with a shorter list of 'immediate' reactions to account for what kind of reactions might actually occur inside the complex. The code starts by identifying if a radical is delocalised or not, and implements the following list of reactions for either the non-delocalised radical or both Lewis structures of the delocalized radical. All three reactions are barrierless according to Vereecken et al. (2004); Vereecken (2008).

1. $R_1{-}C{\cdot}OO{-}R_2 \longrightarrow R_1{-}C{=}O + {\cdot}O{-}R_2$. Barrierless decomposition of peroxides at the radical center.

2. $R{-}C{\cdot}OOH \longrightarrow R{-}C{=}O + {\cdot}OH$. Barrierless decomposition of α-hydroperoxy alkyl radicals into a carbonyl and an OH radical.

3. $R{-}C{\cdot}ONO_2 \longrightarrow R{-}C{=}O + NO_2{\cdot}$. Barrierless decomposition of α-nitrate alkyl radicals into a carbonyl and a nitro radical.

These may not be the only further decomposition reactions that are possible for the product radicals of in-complex RO decomposition reactions. Low-barrier reactions such as decomposition of acyl oxy radicals into alkyl radicals and carbon dioxide ($RC(O)O{\cdot} \longrightarrow R{\cdot} + CO_2$ (Vereecken and Peeters, 2009)) and decomposition of diacyl radicals into an acyl radical and carbon monoxide ($R{-}(C{=}O){-}C{\cdot}{=}O \longrightarrow R{-}C{\cdot}{=}O + CO$ (Méreau et al., 2001)) were also considered but ultimately not included, as these reactions are not barrierless, and may not occur after an endothermic (Orlando et al., 2003) RO decomposition. These downstream decomposition reactions must likely be barrierless to efficiently compete with association of the radical product and the other RO in the ^{3}(RO...OR) complex.

A separate output is written for all the RO reactions that are considered for in-complex branching to help keep track of the accretion products.

2.1.5 Filtering of accretion products

As discussed in Sect. 1.1, the assumption is currently that the RO decomposition reaction is generally followed by recombination of the two radicals into an ether or ester. In the Supplementary of Peräkylä et al. (2023) this assumption was tested for a small model system, where it turned out that this recombination had a high energy barrier in the triplet state, and thus required an ISC. However, this ISC was faster than that of the ^{3}(RO…OR) complex, being on the order of 10^{11} s^{-1}. While a fast dissociation of the two radicals post-RO decomposition can not be entirely ruled out in reality, it is reasonably to assume that dissociation of the product radical and the remaining RO is less competitive than dissociation of the two RO in the ^{3}(RO…OR) complex, especially as RO β-scission reactions are typically endothermic. The GECKO-AP code thus operates on the assumption that the RO decomposition always leads to recombination of the radical product with the second RO in the complex.

The final part of the code cycles through all pairs of RO_2 not filtered out by either the probability or HBN criteria. Branching ratios for all available reaction routes are considered by comparing the reaction rates of both RO and the ISC rate, with the latter assumed to be 10^9 s^{-1} in all cases. Reaction routes are filtered by two criteria: Branching ratio and final yield, which is a combination of recombination yield and branching ratio. Low branching ratios are filtered out using the branching ratio cutoff 0.05, with more tolerance for channels with higher rate uncertainty. The uncertainty factors f used were 1 for β-scissions, 5 for H-shifts and 50 for spin-flips. ~~These~~ The first two of these factors were chosen based on the reported uncertainties in the SARs for these reaction classes: A factor of 2 for the β-scissions (Vereecken and Peeters, 2009), and a factor of 10 for the fastest H-shifts (Vereecken and Peeters, 2010)~~, and a factor of 100 for~~ . The relative uncertainty of the ISC rates ~~based on~~ was determined from the variance in the available computational ISC rates for ^{3}(RO…OR) rates (Hasan, 2023).

In other words, channels were filtered out if:

$$\frac{k_r}{k_{ISC} + \sum_i^{n_\alpha} k_i + \sum_j^{n_\beta} k_j} < \frac{0.05}{f} \tag{6}$$

where n_X is the number of unimolecular reaction channels found for the RO X, whereas k_i and k_j are the rates of said channels. Note that the rates of channels R2 and R3 are neglected by necessity, as we lack ~~the ability~~ a simple way to estimate them ~~adequately~~with the information available to the code. As a final criteria, Equations 2 and 6 are combined into a single inequality with an additional factor of 10:

$$y_{\mathrm{Prod}} = \frac{y_{\mathrm{RO_2RO_2}} \times k_r}{k_{ISC} + \sum_i^{n_A} k_i + \sum_j^{n_B} k_j} < 10 y_c \frac{0.05}{f} \tag{7}$$

where y_c is the same cutoff used to filter RO_2 pairs by recombination probability. This value was adjusted between the three datasets, as seen in the next section. The role of the factor of 10 is to ensure that minor channels are more heavily filtered out

for less likely pairs of RO_2. For the reaction channels that pass all filters, the molecular structure, the molecular mass and the saturation vapour pressure (using two different group additivity methods, SIMPOL (Pankow and Asher, 2008) and Nannoolal (Nannoolal et al., 2004, 2008), the latter with Compernolle's additional -OOH and −C(O)OOH parameters (Compernolle et al., 2010)) are printed out in the output.

As an additional note on the Nannoolal vapour pressures: A previous computational study on the vapour pressures of large ROOR-type accretion products (Kurtén et al., 2016) suggested that the Nannoolal model produces strange results when applied to these molecules. A comparison was performed on the vapour pressures presented in that study with those predicted by the above implementation of the Nannoolal model (See Sect. S4 of the Supplement). Based on this comparison we conclude that the error is likely in the UManSysProp (Topping) implementation of Nannoolal utilized by Kurtén et al. (2016), not in the model itself.

2.2 Data Generation and Curation

2.2.1 Presentation of the Datasets

Three datasets of accretion products with different precursor molecules were produced in order to analyse the most important trends in varying atmospheric conditions. For all runs, a critical vapour pressure value of $p_c = 10^{-13}$ atm was used, meaning that further gas-phase chemistry was not generated for closed-shell molecules with $p_{Sat} < p_c$. The maximum generation of oxidation products and the cutoff value for $y_{\mathrm{RO_2RO_2}}$ were adjusted for each run to ensure that the datasets were kept at a manageable size, and that low-yield downstream products would not be overrepresented in the data. A sensitivity analysis of the y_c parameter is found in Sect. S5 of the Supplement. These three datasets are presented below:

1. The DTA dataset, including the accretion products produced in the atmospheric oxidation of n-Decane, Toluene and α-pinene. The oxidation products generated by GECKO-A for this set of precursor molecules has been studied in detail before (Isaacman-VanWertz and Aumont, 2021; Besel et al., 2023), so a dataset made out of oxidation products previously missing from GECKO-A is a good addition. Accretion products were generated up to the 4th generation and the yield cutoff $y_c = 0.0045$ was used.

2. The Terpene dataset, including the accretion products produced in the atmospheric oxidation of Isoprene, α-pinene, β-pinene, Limonene, β-Ocimene, Sabinene, Δ-3-Carene, and Myrcene. These are the eight most common terpene molecules (Sindelarova et al., 2014). A dataset composed of all the $RO_2 + RO_2$ cross products from these precursors should represent accretion product formation occuring in pristine low-NO_x forest environments reasonably well. Accretion products were generated up to the 2nd generation and the yield cutoff $y_c = 0.003$ was used.

3. The Caryophyllene dataset, including the accretion products from β-caryophyllene, a sesquiterpene for which aerosol particle formation has been recently studied (Dada et al., 2023). Here products were only generated up to the 1st gen-

eration, as some of the 2nd generation accretion products proved unmanageably complex for the mechanism generator. The yield cutoff $y_c = 0.001$ was used.

The isomer switching code presented by Valorso et al. (2011) was turned off during the runs to ensure the traceability of the RO_2 formation mechanisms. $RO_2 + OH$ reactions were also turned off when generating these datasets, as ~~the current paramerization in GECKO-A this reaction most often leads to~~ this leads to the formation of hydrotrioxides (ROOOH) ~~, chemistry includes several unknown details. Based~~ in the current parametrization of GECKO-A. The chemistry of these molecules is not well-known, but based on known decomposition and OH oxidation rate coefficients for CH_3OOOH and Isoprene derived ROOOH, (Assaf et al., 2018; Anglada and Solé, 2018; Berndt et al., 2022), we are not able to completely neglect other OH or O_3 oxidation pathways of hydrotrioxides, ~~whose chemistry we have virtually no knowledge on~~both of which we lack systematic data for. Fortunately, with a typical atmospheric OH concentration of 10^6 molecule cm^{-3} (Wayne, 2000) the $RO_2 + OH$ channel will often be outcompeted by the other channels, so ignoring them is not a massive loss in chemical accuracy.

2.2.2 Dataset Curation

Additional GECKO-A mechanisms without the GECKO-AP code were generated for each set of precursor molecules to supply the datasets with additional metadata. Six mechanisms were generated with a limited set of VOC oxidants (only OH, only O_3, only NO_3, OH+O_3, OH+NO_3, and O_3+NO_3, respectively). Each RO_2 in the accretion product datasets was assigned a required combination of atmospheric oxidants based on the RO_2 list resulting from these mechanisms. Similarly, for the DTA and Terpene datasets a GECKO-A mechanism was generated for each product generation leading up to the final one to assign a generation to each of the RO_2 in the dataset. Finally, for each precursor molecule in the DTA and Terpene datasets a mechanism was generated with only one precursor in to label which of the precursors each of the RO_2 is derived from. Based on this RO_2 labelling, a final probability-based filtering criteria was applied to all datasets, as OH and NO_3 are known to rarely have simultaneously high concentrations, as the former is produced by photolysis of O_3 while the latter is decomposed by photolysis (Seinfeld and Pandis, 2016). For this reason the cross reactions of OH-derived RO_2 and NO_3-derived RO_2, along with all their products, were removed from the data. Care was taken to not accidentally remove radicals produced from both oxidation mechanisms (for example products of H-abstraction). By the same logic, RO_2 with formation mechanisms requiring OH oxidation of a VOC in one generation and NO_3 oxidation in the next (or vice versa) were also removed. Admittedly these mechanisms are more plausible than cross reactions of OH-derived RO_2 and NO_3-derived RO_2 if the lifetimes of the 1st generation closed-shell products exceed the diurnal cycle, but nevertheless it is likely that the GECKO-A mechanism generator overestimates the yields of these radicals relative to all other RO_2.

For the purpose of data analysis four versions of the final data was created for each dataset: The 1st contains all the reaction channels found by the code, including those removed by the OH+NO_3 criteria. This data isn't analysed separately in this work, but it is distributed as a reference. In the second version of data, the OH+NO_3 products have been removed, but nothing else.

This version is analysed in Sect. 3.3. In the third version all of the non-accretion products are removed (analysed in Sect. 3.4) and in the fourth version all the duplicate accretion products are removed. ~~(The causes for these are discussed below in Sect. ??)~~ This last version is only used for the figures in Sect. 3.2 and Sect. S6 of the Supplement, but the existence of such uniqueness-filtered datasets was considered useful for potential follow-up studies such as the analysis performed by Besel et al. (2023) for the data presented by Isaacman-VanWertz and Aumont (2021).

2.2.3 ~~Duplicate Products~~

2.3 Estimation of Atmospheric concentrations

~~Several reaction channels resulted in identical accretion products. An analysis of the data identified two causes for this, not including the trivial case of decomposition product symmetry in RO_2 self-reactions.~~ ~~**Fragment radical symmetry**~~ ~~occurs when decomposition reactionsof different alkoxy radicals result in the same radical fragment, all of which can recombine with the same alkoxy radical to form the same accretion product. This is especially common if the fragment radical is small. For example, the $CHO\cdot$, $CH_3CO\cdot$, $\cdot C(O)OOH$ and $\cdot CH_2OOH$ radicals were formed from over 200 found RO reactions each in the DTA dataset. This effect is responsible for the majority of all duplicate molecules encountered in the raw output. The second category,~~ ~~**chemical pathway crossing**~~~~, is our term for all other duplicate products found in the data. These duplicates often seem to be caused by many of~~ In order to explore the impact of accretion product formation from $RO_2 + RO_2$ reactions, RO_2 concentrations were calculated for representative conditions of biogenic environments where the $RO_2 + RO_2$ reactions are expected to be relatively important. RO_2 concentrations were calculated from the numerical solution of the kinetic steady-state equations (Equation 8) based on the reactions in the ~~peroxy radicals in the code stemming from the same parent VOC,~~ GECKO-A mechanism. Furthermore, the mechanism was limited to Isoprene oxidation and includes only the 1st and ~~therefore often being only a few bond scissions or formations removed from each other in chemical space. This being the case, different combinations of distinct peroxy radicals with different RO decomposition channels sometimes result in identical accretion products by coincidence. The occurrence of these symmetries can be considered a property instrumental to GECKO-AP, since it only considers 'vertical' oxidation reactions for one parent compound while neglecting bimolecular reactions of organic oxidation products.~~ 2nd generation radicals (7 581 reactions). First however, a representative set of bimolecular reactant concentrations was chosen based on balancing a simpler set of steady-state equations, with only CH_4, CO, CH_2O and CH_3OH present as organic precursors. The criteria used to find the ideal $RO_2 + RO_2$ conditions was based on the GEOS-Chem-modelled probability distributions presented by Kenagy et al. (2024), according to which a $\frac{k_{RO_2NO}[NO]}{k_{RO_2NO}[NO]+k_{RO_2HO_2}[HO_2]}$ value of 0.2 corresponds to both a $\frac{[RO_2]}{[HO_2]}$ ratio well above 1 and a not insignificant probability density. Assuming the $RO_2 + NO$ and $RO_2 + HO_2$ rates are approximately similar for typical RO_2, we thus balanced the steady-state equations for OH, O_3, HO_2, NO, NO_2, and NO_3 aiming for a $\frac{[NO]}{[NO]+[HO_2]}$ ratio of 0.2.

$$\frac{dc}{dt} = Sources - Sinks \cdot c \approx 0 \implies c \approx \frac{Sources}{Sinks} \tag{8}$$

As the probability distribution of Kenagy et al. (2024) was weighted by Isoprene + OH, it likely over-represents daytime conditions, as both Isoprene and OH concentrations peak during the day (Wennberg et al., 2018). We thus re-balanced the steady-state equations with no photolysis reactions present, using the diurnal cycles presented by Bey et al. (1997) as reference. The resulting day- and nighttime concentrations of OH, O_3, HO_2, NO, NO_2, and NO_3 were treated as constants in the steady-state equations for the Isoprene-RO_2. A (constant) Isoprene concentration of 10^{11} molecule cm^{-3} was used for daytime and 10^{10} molecule cm^{-3} for nighttime. The temperature $T = 298$ K was used for both. Full details of how the steady-state equations were solved are found in Section S8 of the Supplement.

3 Results and Discussion

3.1 Competitive decomposition channels

First, we use the β-scission and H-shift SARs (Vereecken and Peeters, 2009, 2010) to assess which of the reaction channels described in Sect. 2.1.4 are fast enough to occur in ^{3}(RO…OR) complexes.

Assuming a constant ISC rate of 10^9 s^{-1}, the β-scission rate must presumably be at least 10^8 s^{-1} in order for the product yield to be non-negligible. With Vereecken's suggested constant A-factor of $1.8 \cdot 10^{13}$ s^{-1}, an activation barrier below 30 kJ/mol is needed to reach this rate at 298 K, which means 44.9 kJ/mol worth of activating factors from the SAR's base value of 74.9 kJ/mol. The only activating factors to reach this barrier reduction single-handedly are the α-O group (present in all $RC(O)O_2 + RO_2$ reactions), the β-NO group (not present in our data), and opening of 3- and 4-membered rings. (relevant for both Pinenes, Sabinene & Δ-3-Carene -derived RO_2) Other activating factors that are frequently present in our generated RO_2 are β-C=O, (leading to the formation of ester accretion products) β-OOH, β-OH, β-C=C, and opening of 5- and 6-membered rings. In summary, there is no shortage of chemical structures present in atmospheric RO_2 that lead to competitive RO β-scission reactions. Interestingly, all of the most competitive β-scission seem to be of the ring-opening type, which may partially explain why these reactions have eluded detection for so long. Exocyclic β-scissions have two products, whereas endocyclic scissions have one. Only the former is distinguishable from the ROOR in the mass spectrometric measurements which have thus far been the detection method of choice for highly oxidized organics in atmospheric chemistry (Ehn et al., 2014; Rissanen et al., 2014; Bianchi et al., 2019).

Type	Span	H	k_{H} (s^{-1})
α-OH	1,5	CH	$7.0 \cdot 10^7$
α-OH	1,6	CH	$4.7 \cdot 10^7$
>C(OH)O·	1,5	CH	$4.1 \cdot 10^7$
Aldehyde H	1,5	CHO	$2.9 \cdot 10^7$
α-OH	1,5	CH_2	$2.1 \cdot 10^7$
Exo-β-OH	1,5	CH	$2.0 \cdot 10^7$
α-OH	1,6	CH_2	$1.4 \cdot 10^7$
>C(OH)O·	1,5	CH_2	$1.2 \cdot 10^7$

Table 2. A list of the RO unimolecular H-shift which might be fast enough to occur in $^3(\mathrm{RO}\ldots\mathrm{OR})$ complexes according to Vereecken's SAR. (Vereecken and Peeters, 2010)

For the unimolecular H-shifts, the list of potentially competitive reactions is considerably shorter, as no H-shift has rates above 10^8 s^{-1} in the SAR. However, as these rates are uncertain by a factor of 10 (Vereecken and Peeters, 2010), the reactions with rates above 10^7 s^{-1} are still worth considering, especially as rates above 10^8 s^{-1} have been reported. (Orlando et al., 2003) The unimolecular H-shift reactions above this rate threshold are listed in Table 2.

Overall, it is notable that the in-complex decomposition channels outnumber the ISC channels in the data 142 009 to 79 833 in the DTA dataset and 161 784 to 129 585 in the Terpene dataset. The ISC channels also have lower yields on average, accounting only for 22.1 % of the total yield of products from 1st generation radicals in the DTA dataset and 35.4 % in the Terpene dataset. These yields should be treated with a grain of salt, considering the large amount of simplifications done when applying the filtering criteria, but they do offer some indication that these in-complex RO decomposition channels are common, and become increasingly competitive with more complex RO intermediates.

3.2 Statistics on Molecular Properties

The distribution of RO_2 by rate classes are presented in Table 3 for the DTA dataset and in Table 4 for the Terpene and β-Caryophyllene datasets. One detail of note in the latter is that Isoprene seems to almost exclusively generate RO_2 with fast $RO_2 + RO_2$ rates. This implies that Isoprene-derived RO_2 ~~punch above their weight~~ contribute more than expected from their concentration when it comes to RO_2 recombination yields. Out of the seven monoterpenes treated in the data, Limonene clearly produces the largest diversity of RO_2, owing to having both an endocyclic and an exocyclic C=C bond. We also see from both tables that the production of tert-RO_2 molecules is mostly dependent on the existence of tertiary double-bonded carbons, which is largely unsurprising.

As atmospheric oxidation proceeds, the reactant RO_2 get increasingly fragmented and oxidized. This is showcased for the radicals in the DTA dataset in Figure 2 and for the Terpene and β-Caryophyllene datasets in Figure 3. For the formed accretion products, the distribution of the same properties is presented in Figures 4 and 5. As our methodology might be overemphasizing

Gen	Prec.	Tot	1	3	4	5	7	8	9	OH	O_3	NO_3 ~~⟨Yield⟩~~
1st	Dec	~~11~~ 10	0	0	9	0	1	0	~~1~~ 0	~~11~~ 10	0	10 ~~24.6 %~~
2nd	Dec	~~219~~ 208	0	0	112	0	~~86~~ 83	~~4~~ 1	~~17~~ **12**	~~188~~ 179	0	~~162 3.3 %~~ 156
3rd	Dec	~~261~~ 233	0	0	~~82~~ 79	0	~~138~~ 119	~~13~~ 9	~~28~~ 26	~~203~~ 177	0	~~126 2.6 %~~ 119
4th	Dec	~~224~~ 242	0	0	~~55~~ 53	0	~~125~~ 133	~~13~~ 19	~~31~~ 37	~~201~~ 213	0	~~94 1.2 %~~ 102
1st	Tol	~~15~~ 12	0	0	4	1	1	~~5~~ 3	**4** 3	~~15~~ 12	~~1~~ 0	~~2 28.9 %~~ 1
2nd	Tol	~~138~~ 123	0	8	12	2	~~44~~ 41	~~28~~ 24	~~44~~ **36**	~~162~~ 123	~~24~~ 14	~~11 11.0 %~~ 2
3rd	Tol	~~386~~ 345	0	~~25~~ 24	20	5	~~125~~ 106	~~83~~ 73	~~128~~ 117	~~367~~ 345	~~47~~ 31	~~33 8.0 %~~ 1
4th	Tol	1 ~~168~~ 070	0	~~134~~ 121	~~21~~ 26	~~3~~ 8	~~508~~ 440	150	~~352~~ 325	1 ~~099~~ 070	~~264~~ 147	~~182 5.1 %~~ 4
1st	α-pin	60	8	5	14	0	17	7	**9**	26	28	8 ~~11.0 %~~
2nd	α-pin	~~563~~ 554	~~94~~ 92	~~99~~ 97	~~62~~ 61	2	~~189~~ 187	43	~~74~~ 72	~~419~~ 413	~~306~~ 303	~~278 5.2 %~~ 270
3rd	α-pin	1 ~~642~~ 566	~~168~~ 162	~~424~~ 406	~~88~~ 86	0	~~520~~ 495	~~176~~ 168	~~266~~ 249	1 ~~109~~ 033	1 ~~027~~ 004	~~962 3.1 %~~ 922
4th	α-pin	2 197	~~124~~ 122	~~731~~ 722	~~41~~ 42	0	~~661~~ 671	~~223~~ 225	~~417~~ 415	1 ~~607~~ 622	1 ~~338~~ 376	1 ~~134 1.9 %~~ 13

Table 3. The number of peroxy radicals per generation, ~~precursor,~~ recombination rate class and oxidant for each precursor molecule in the DTA dataset. For an explanation of the classes, refer to Table 1. The oxidant labels are defined inclusively (H-abstraction RO_2 with the label 'OH~~+~~,NO_3' are included in both columns).

accretion products in later generations (See Sect. S5 of the Supplement), all RO_2 are grouped by the generation where they first form, and all accretion products are labelled 'Gen n+m', where n and m are the generations of the two reacting RO_2. We also present histograms where each accretion product is weighted by our best proxy for the formation rate, which is the product of the $RO_2 + RO_2$ recombination rate (Eq. 3) and the in-complex branching ratio (Eq. 6). With this weighting we neglect the relative importance of individual RO_2 radicals, as the theoretical maximum yields are not fully comparable. Comparing the carbon number distributions of accretion product and RO_2 radical scaled yields in Fig 5b to the corresponding radicals in Figure 3b, we notice an interesting trend in both the monoterpene and sesquiterpene results: the largest peak of accretion products occurs at C atom numbers only slightly larger than the bulk of the RO_2. In the Terpene dataset all of the major 1st generation RO_2 have 10 C atoms, but the largest peak in accretion product yield is at 11 and 12 C atoms rather than 20. The same is seen in the β-caryophyllene dataset where the RO_2 yield peaks at 13-15 C atoms whereas the accretion product yield peaks at 14-17. However, the explanations for this phenomenon seem to differ between the two datasets. In the β-caryophyllene data 73 % of this yield peak comes from cross reactions of ~~MetC(O)O$_2$~~ $CH_3C(O)O_2$ with the C_{13-15} radicals, in the Terpene dataset this number is only 30 %. On the other hand, 38 % of this yield comes from fragmentations of larger RO_2 + RO_2 pairs, and the rest simply come from recombinations of RO_2 with smaller C atom numbers. This underlines the importance of the $RC(O)O_2$ for accretion product formation, as they, at least in the Jenkin et al. (2019) parametrization, react rapidly even with the largest and most sterically hindered tert-RO_2.

Gen	Prec.	Tot	1	3	4	5	7	8	9	OH	O_3	NO_3
1st	Iso	27 18	0	0	0	4	5	7	10 2	6 19 9	19 4	35.8 % 5
2nd	Iso	123 125	0	29 25	0	1	45 43	31 35	17 21	80 87	46 54	58 12.0 %
1st	α-pin	76 70	10 9	5	15	1	23 22	11 9	**11 9**	54 34	36 28	18 15.3 %
2nd	α-pin	685 682	115 116	127 124	73	2	233 230	53 54	82 83	544 538	371 381	326 4.9 % 3
1st	β-pin	52 46	5	3 2	10	0	18 17	6 4	**10 8**	33 17	22 14	27 32.5 %
2nd	β-pin	697 706	122	95	104 103	0	242 248	45 52	89 85	475 485	276 275	380 5.4 %
1st	Lim	79 60	2	5	15 10	6	27 19	15 12	**9 6**	45 22	59 50	31 21.3 %
2nd	Lim	1 043 062	27	228 227	76 81	73	335 343	196 201	108 110	712	735 762	253 5.1 % 2
1st	β-oci	39 26	4	2	3 2	5 4	8 6	9 5	**8 3**	29 12	23 10	21 26.5 %
2nd	β-oci	382 380	8	78 69	10 11	44 46	129 125	91 94	22 27	278 279	198 219	113 6.9 %
1st	Sabi	59 54	11	8	5	0	23 21	4 2	**7 6**	37 23	15 10	31 21.5 %
2nd	Sabi	520 519	81	94	28	0	198 195	41 42	78 **79**	308	182 178	316 4.8 % 3
1st	Δ-3-car	33 28	3	3	7	0	11 10	4 1	**5 4**	27 22	13 6	11 24.0 %
2nd	Δ-3-car	311 298	30 29	37 34	19	0	127 124	46 44	52 48	241 229	138 140	116 7.6 % 1
1st	Myr	51 35	3 2	2	4	7 6	15 11	14 9	**6 1**	41 24	15 5	23 23.5 %
2nd	Myr	564 565	9	96 93	27	61 63	205 202	118 119	48 52	424 425	207 231	171 6.2 % 1
1st	β-Car.	179	39	11	28	17	49	17	**18**	38	110	36 4.2 %

Table 4. The number of peroxy radicals per generation, ~~precursor,~~ recombination rate class and oxidant for each precursor molecule in the Terpene and β-caryophyllene datasets. For an explanation of the classes, refer to Table 1. The class 9 number is bolded if it includes ~~MetC(O)O$_2$~~$CH_3C(O)O_2$.

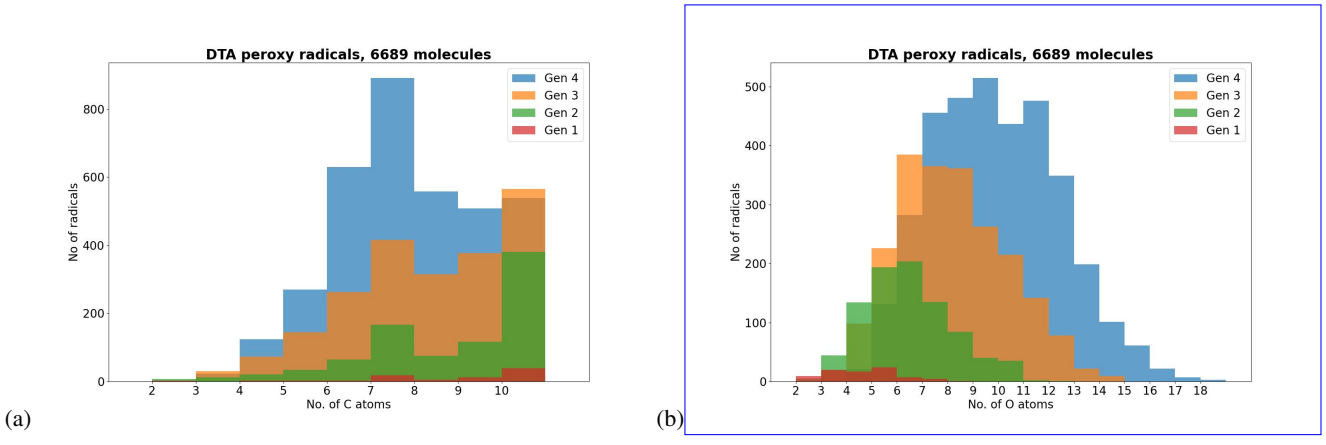

(a) (b)

Figure 2. The RO_2 in the DTA dataset by number of C and O atoms, the latter including the RO_2 functionality.

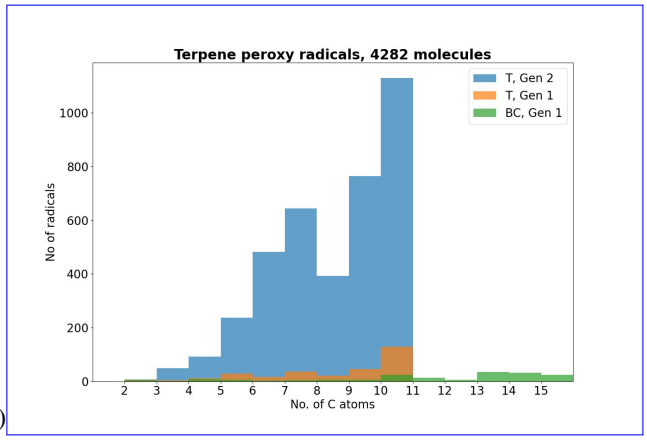

(ea)

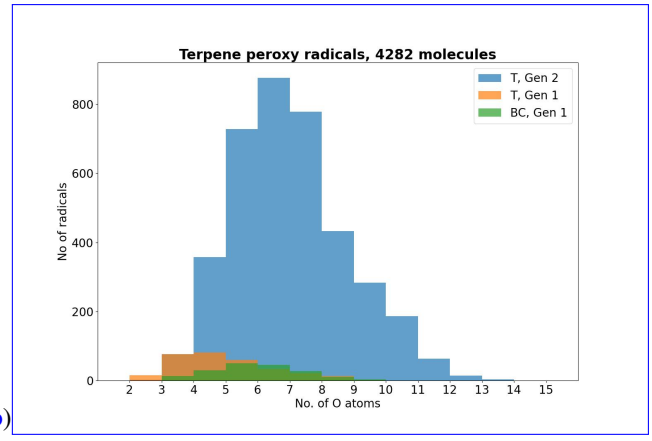

(db)

Figure 3. The ~~RO_2~~ peroxy radicals in the ~~DTA dataset~~ Terpene and β-Caryophyllene datasets by number of C and O atoms, the latter including the RO_2 functionality. ~~Figures (b) & (d) are weighted by theoretical maximum yield, with each generation scaled such that the sum of all RO_2 yields per generation is 1.~~

The distribution of functional groups in the RO_2 and (unique) accretion products are shown in Figure 6. When comparing the two figures we see that the number of accretion products with either ether or ester functionalities is less than those with a peroxide functionality, and this is only partially explained by the presence of peroxides in the DTA RO_2. This is likely due to the fact that there are more duplicates among the ether and ester products. The average in-complex branching ratio of all the ISC products remaining after filtering is 33.5 % in the DTA dataset and 36.6 % in the Terpene dataset, again implying that the total yield of ether and ester products is typically higher. Interestingly, aromatic rings are highly represented in the DTA accretion products. The reason for this seems to be instrumental: The aromatic RO_2 in the data all have high yields due to being directly derived from the 1st H-abstraction product $Ar-CH_2O_2$, which has a yield of 100 % from NO_3 oxidation of Toluene. Of course, H-abstraction from a methyl group by NO_3 is a slow reaction (Kerdouci et al., 2010), meaning that Toluene + NO_3 might in reality not effectively be the dominant reaction even in favourable conditions. This detail is another example of why our results ought to be treated as qualitative rather than quantitative.

(a)~~(b)(c)(d)The peroxy radicals in the Terpene and β-Caryophyllene datasets by number of C and O atoms, the latter including the RO_2 functionality. Figures (b) & (d) are weighted by theoretical maximum yield, with each generation scaled such that the sum of all RO_2 yields per generation is 1.~~

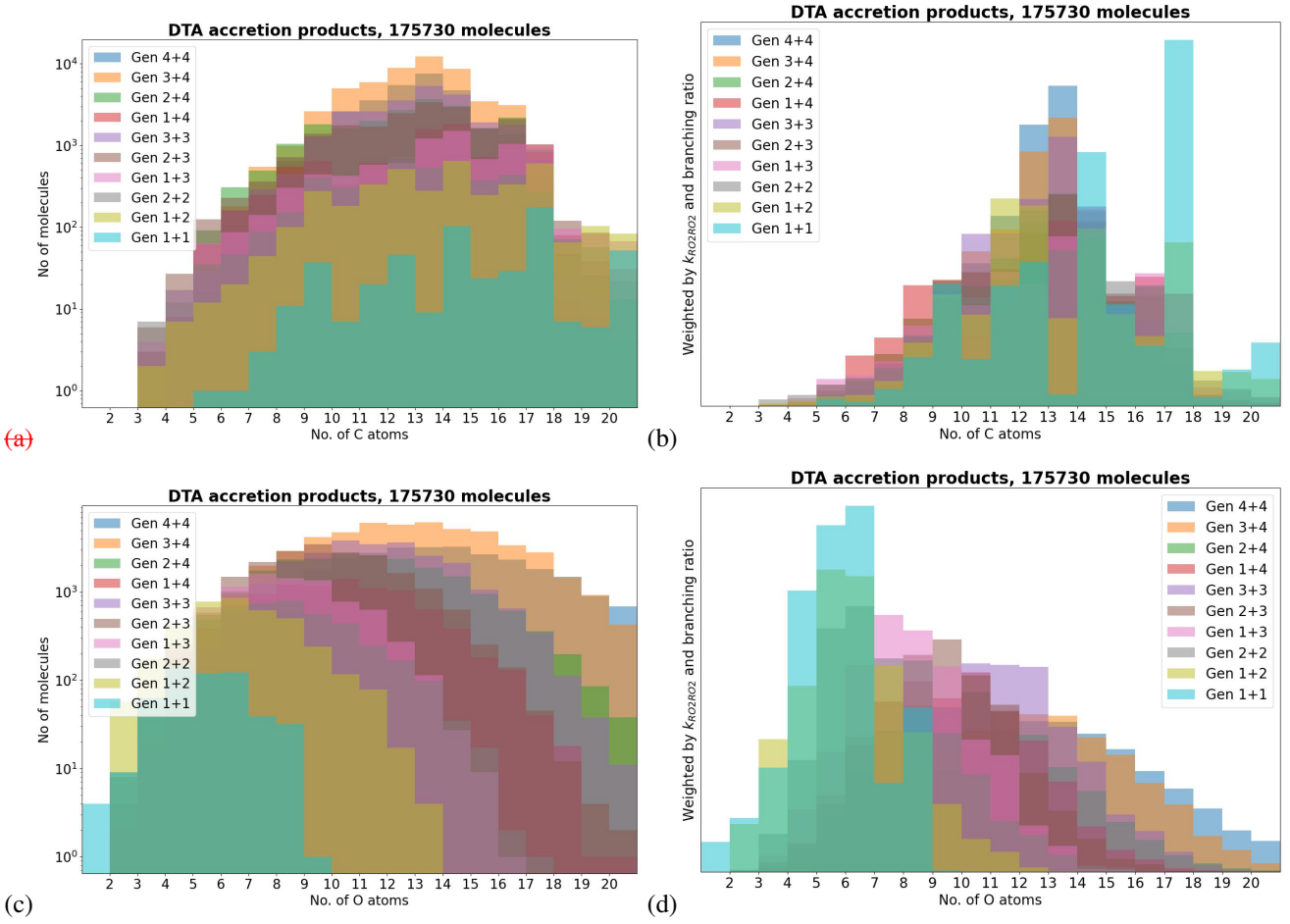

Figure 4. The accretion products in the DTA dataset by number of C and O atoms.~~Figures (b) & (d) are weighted by theoretical maximum yield, with each generation scaled such that the sum is 1 for each generation combo.~~

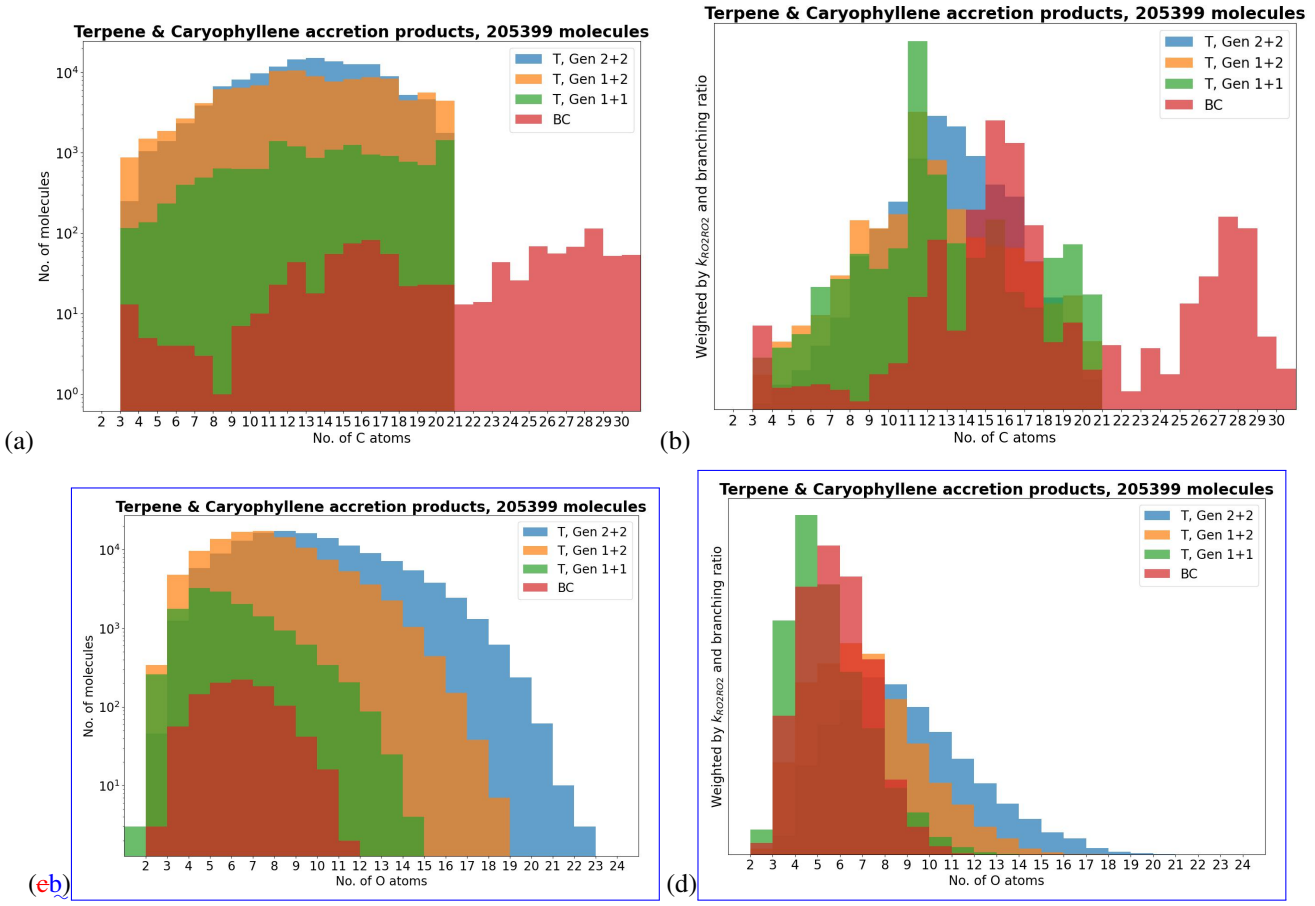

Figure 5. The accretion products in the Terpene and β-Caryophyllene datasets by number of C and O atoms. ~~Figures (b) & (d) are scaled by theoretical maximum yield, with each generation scaled such that the sum is 1 for each generation combo~~'BC' = β-Caryophyllene.

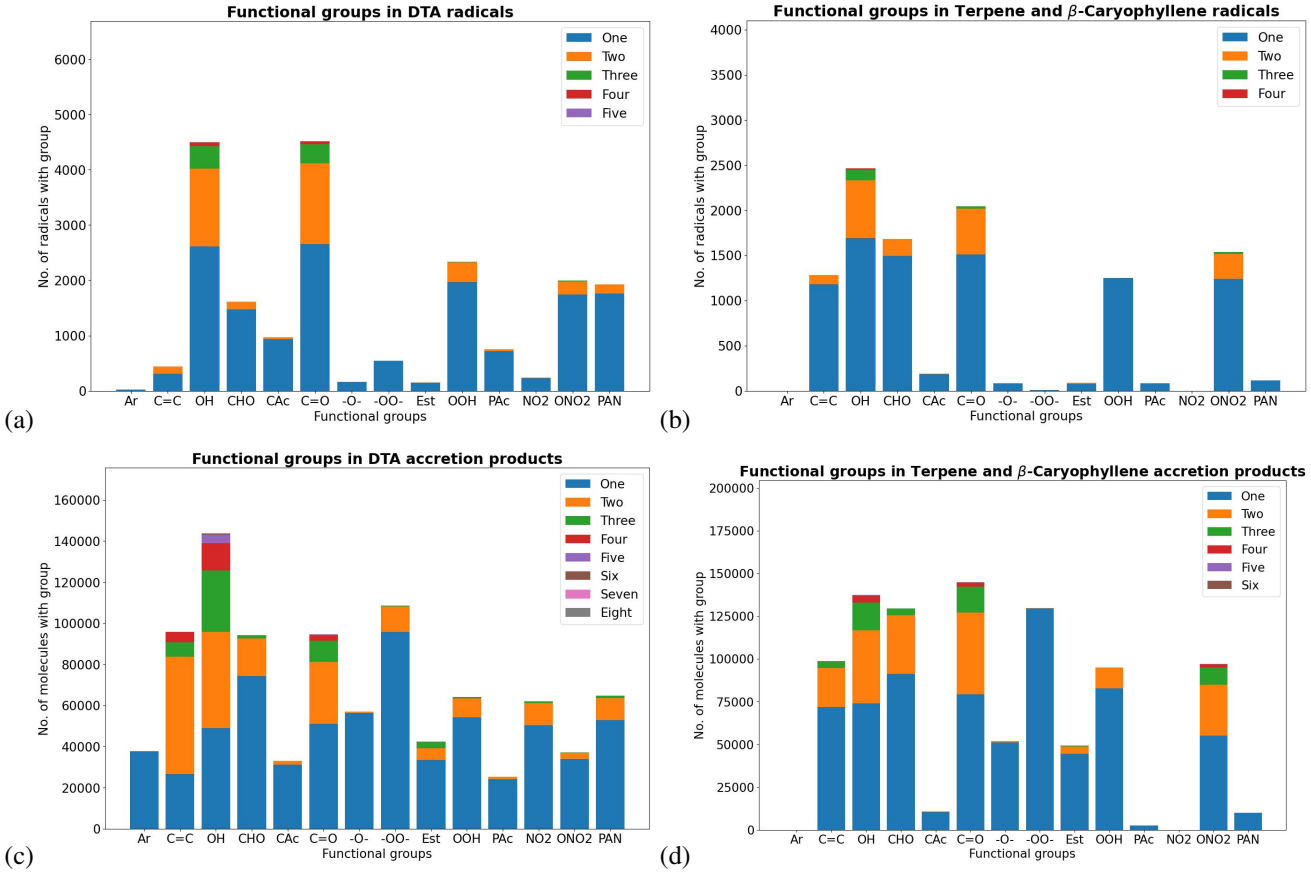

Figure 6. The distribution of functional groups in the in the DTA and Terpene datasets for the RO_2 (a) & (b) as well as the (unique) accretion products (c) & (d). CAc: Carboxylic Acid, C(O)OH. Est: Ester, C(O)OC. PAc: Peroxy acid, C(O)OOH PAN: Peroxy acyl nitrate, $C(O)OONO_2$.

3.3 Accretion product inhibiting reactions

Since we have presented a new channel for accretion product inhibition, namely the alkoxy radical decomposition reaction leading to ejection of either a OH or NO_2 radical, we should analyse the extent to which these inhibiting reactions occur in the data. This was done exclusively on the DTA dataset, due to the generally higher oxidation states of its RO_2 resulting in more competitive RO decompositions. The simplest type of inhibition reaction is the α-nitro ejection, which in the code insures that peroxy radicals with an NO_2 group in ~~α-position~~ the geminal position never form accretion products. As shown by our computational reaction rates in Sect. S3 of the Supplement, this is not necessarily always be the case in reality, but the α-NO_2 ejection ought to still be among the most competitive channels. This is our first accretion product inhibiting reaction, and it can be treated as a given rule. The reaction is presented in the following scheme:

$$\begin{aligned} \mathrm{R_1(NO_2)O_2\cdot + R_2O_2\cdot} &\longrightarrow \mathrm{(R_1(NO_2)O\cdot\ldots\cdot OR_2) + O_2} \\ \mathrm{R_1(NO_2)O\cdot} &\longrightarrow \mathrm{R_1{=}O + \cdot NO_2} \\ \mathrm{(R_1{=}O\ldots\cdot NO_2\ldots\cdot OR_2)} &\longrightarrow \mathrm{R_1{=}O + R_2ONO_2} \end{aligned}$$

These α-NO_2 radicals all form downstream from Toluene oxidation pathways in the DTA dataset. The reaction channel responsible for these is NO_2 addition to aryloxy radicals. ($\mathrm{Ar{-}O\cdot + NO_2} \longrightarrow \mathrm{Ar(ortho{-}NO_2)OH}$, Platz et al. (1998)) Thus these peroxy radicals and the associated (RO…OR) complexes were left out from the following analysis.

The second reaction inhibiting the accretion product formation is the barrierless decomposition of α-hydroperoxy alkyl radicals, a reaction channel that is possible for all peroxy radicals with -OOH substituents. The inhibition is presented in the following scheme, in which R_{OOH} is a OOH-substituted carbon chain:

$$\begin{aligned} \mathrm{R_1O_2\cdot + R_{OOH}O_2\cdot} &\longrightarrow \mathrm{(R_1O\cdot\ldots\cdot OR_{OOH}) + O_2} \\ \mathrm{R_{OOH}O\cdot} &\longrightarrow \mathrm{R_2\cdot OOH} \longrightarrow \mathrm{R_2{=}O + \cdot OH} \\ \mathrm{(R_1O\cdot\ldots\cdot OH\ldots R_2{=}O)} &\longrightarrow \mathrm{R_1OOH + R_2{=}O} \end{aligned}$$

where the reaction step $\mathrm{R_{OOH}O\cdot} \longrightarrow \mathrm{R_2\cdot OOH}$ may be either a β-scission or a unimolecular H-shift. As a measure of the competitiveness of RO reactions leading to this inhibition channel, the average branching ratio as a function of the combined number of OOH groups in the RO_2 pair is shown in Figure 7 (a), both weighted and unweighted by the pair's recombination yield. As we see, the inhibition of accretion product formation increases significantly with the number of hydroperoxide groups.

Our third and final inhibition reaction is the barrierless decomposition of α-nitrate alkyl radicals, a very similar reaction to the corresponding -OOH reaction.

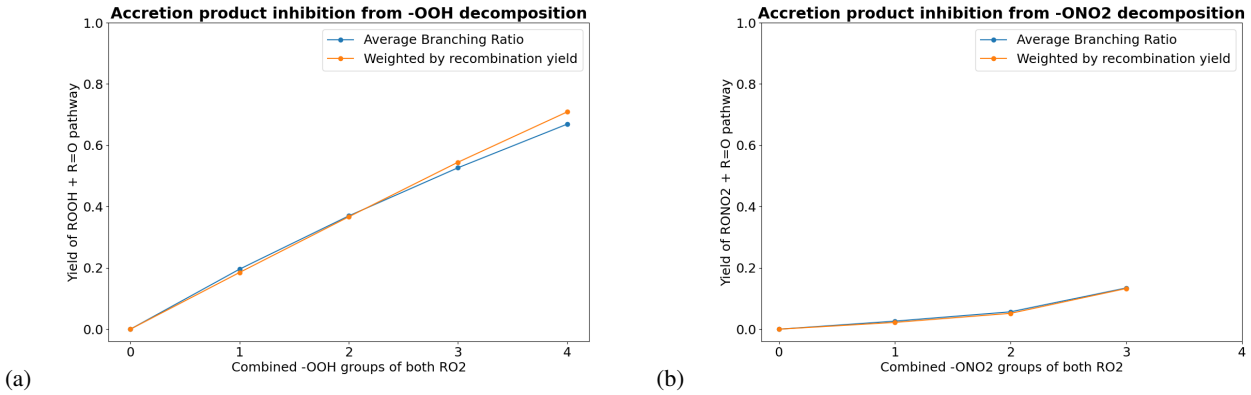

Figure 7. The impact of barrierless $C\cdot OOH$ and $C\cdot ONO_2$ decomposition on formation of accretion products. (a) The average branching ratio of RO reactions leading to $C\cdot OOH$ decomposition by the combined number of -OOH groups in the complex. (b) The same for RO reactions leading to $C\cdot ONO_2$ decomposition. The results for $n = 4$ are excluded because there was only one such RO_2 pair in the data.

$$R_1O_2\cdot + R_{ONO2}O_2\cdot \longrightarrow (R_1O\cdot \ldots \cdot OR_{ONO2}) + O_2$$
$$-R_{ONO2}O\cdot \longrightarrow R_2\cdot ONO_2 \longrightarrow R_2{=}O + \cdot NO_2$$
$$(R_1O\cdot \ldots \cdot NO_2 \ldots R_2{=}O) \longrightarrow R_1ONO_2 + R_2{=}O$$

The average branching ratio of these reactions is presented in Figure 7b.

As seen in a comparison of Figure 7a and b, the hydroperoxide decomposition channel has a significantly higher inhibition yield compared to the nitrate decomposition channel. As most of the competitive alkoxy radical decomposition channels are β-scissions, the explanation for this observation can be found from the group contribution parameters in Vereecken & Peeters's β-scission SAR (Vereecken and Peeters, 2009): If the alkoxy radical has a hydroperoxide group in the β-carbon, the activation energy is lowered by 38.9 kJ/mol. On the other hand, a nitrate group in the β-carbon only lowers the activation energy by 11.7 kJ/mol. Plugging in this difference into an Arrhenius expression ($e^{\frac{27.2\,\frac{kJ}{mol}}{RT}}$) tells us that β-scission reactions leading to the formation of α-OOH alkyl radicals and to ejection of an OH radical will typically be 10^4 times faster than those leading to the ejection of a NO_2 radical, and thus more likely to be competitive. What this means in terms of atmospheric conditions is that highly ONO_2-substituted peroxy radicals forming in high NO_x conditions have a slightly lower chance of forming organic accretion products from RO_2 recombination reactions compared to other sufficiently oxidized RO_2, while highly OOH-substituted peroxy radicals, for example those forming in high HO_2 conditions, have a yet lower chance. Even more importantly, peroxy radical autoxidation is also known to form products with multiple -OOH groups (Bianchi et al., 2019). Autoxidation reactions are currently missing from GECKO-A, so it is unclear how well the highly -OOH substituted RO_2 in the data correspond to those formed from autoxidation reactions. Considering the fact that the inhibition is primarily driven by fast β-scissions in the data, it is particularly notable that optimal RO_2 H-shift span is 1,5 or 1,6 rather than 1,4 (Vereecken and

Nozière, 2020). This suggest that -OOH groups originating from autoxidation may be less likely to be in β-position relative to the alkoxy carbon. For autoxidation-derived RO_2, the inhibition yield may thus increase less steeply compared to Fig. 7.

3.4 Analysis of Vapour Pressure Distributions

As our main interest for accretion products comes from the formation of large low-volatility organic molecules, it is a worthwhile exercise to analyse the vapour pressure distribution of the predicted products. However, as the amount of data produced is rather large, this section will only discuss and visualise the observed main trends. Sect. S6 and S7 of the Supplement features more figures and tables on the vapour pressure distribution of the products. In addition to grouping the products by generation of radicals, they are also grouped by reaction channel, precursor molecule and required VOC oxidants (OH, O_3 and NO_3) to better identify which reaction channels lead to the lowest-volatility products.

3.4.1 Distribution by Reaction Channel

The vapour pressure distribution of ~~the early generation~~ all the accretion products in the DTA and Terpene datasets categorized by reaction channel is presented in Figure ~~??. An alternative visualization including the full data from the DTA and Terp datasets is shown in the Supplement.~~ 8. A few interesting trends pop up when viewing the data this way. First, the vapour pressure distribution of the exocyclic β-scission products is shifted towards higher p_{Sat} values relative to the ISC products. This makes sense, as these products are more fragmented than their ROOR counterparts. This adds an interesting element to the suggestion by Peräkylä et al. (2023) that the ether and ester accretion products contribute more to aerosol particle growth thanks to their higher (thermal) stability. This increased stability often comes at the price of increased volatility, especially if the radical product of the β-scission is relatively small. In other words, these reactions may not always contribute more to aerosol particle growth compared to the ROOR product. On the other hand, the vapour pressure distribution of the endocyclic β-scission products is shifted towards lower p_{Sat} values, meaning that the same trade-off between stability and (low) volatility is not present. The reason for this is somewhat obvious: Endocyclic β-scissions do not fragment the molecule. The same is true of the unimolecular H-shift products, (which in theory ought to be even less volatile as the reaction gives the product an additional OH-group) but these products are less common due to the lower reaction rates (at least in the SAR). As seen when comparing the results between the three datasets, the different molecular structures present do not have a massive impact on the noted differences between the reaction types, but the ratio of exocyclic and endocyclic β-scissions obviously depends on the ring structures and positions of C=C bonds in the precursor VOC.

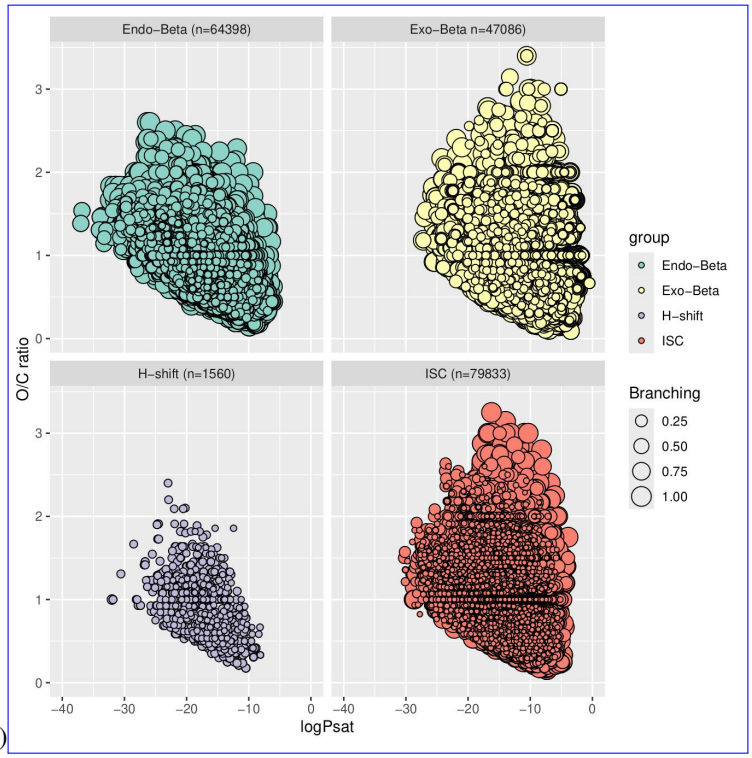

(a)

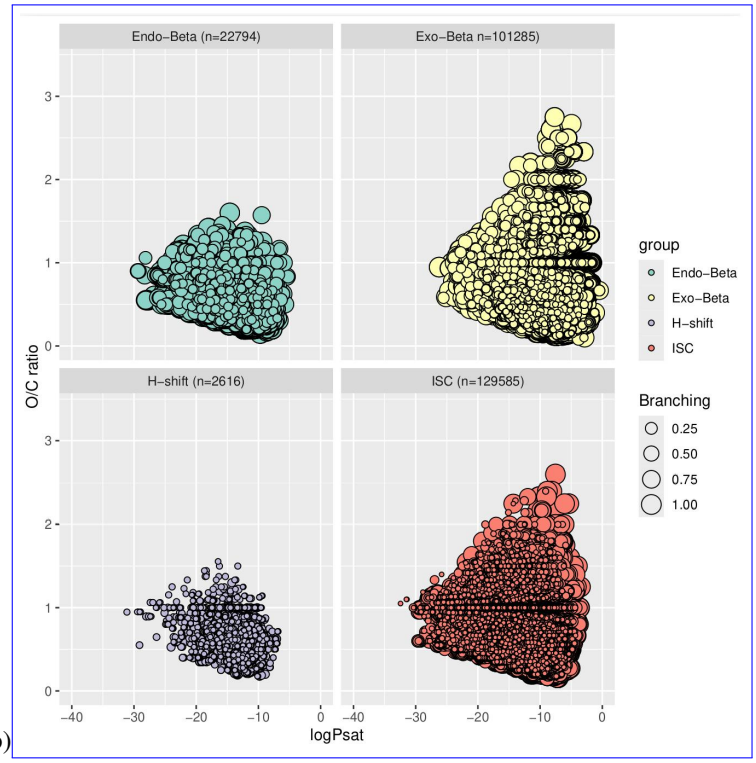

(b) ~~(c)(d)(e)(f)~~

Figure 8. ~~p_{Sat}-distributions~~ A bubble plot of the ~~early generation~~ p_{Sat}-distribution of all accretion products ~~in each dataset~~ categorized by reaction channel ~~.~~ for (a) ~~& (b) Vapour pressure distribution in~~ the DTA ~~datset.~~ dataset and (eb) ~~& (d) Vapour pressure distribution in~~ for the Terpene dataset. ~~(c) & (f) Vapour pressure distribution in the β-Caryophyllene dataset. (b), (d), & (f) are weighted by the product yields.~~ p_{Sat} is expressed in atm.

3.4.2 Distribution by Precursor Molecule

If endocyclic β-scissions are indeed the key to forming low volatility ether and ester products, then the next question is which chemical structures present in the data are especially efficient at forming endocyclic RO_2 in high yields. This is however not the only important factor when it comes to the formation of accretion products, as endocyclic RO_2 tend to be on the lower end of the scale in terms of self-reaction rates, as they are by definition either secondary or tertiary RO_2 (See Table 1). Thus, simultaneously producing large numbers of rapidly reacting $RC(O)O_2$ or primary RO_2 with activating groups may also enhance accretion product formation from the endocyclic RO_2, as the cross reactions between these will be faster than the self-reactions of the endocyclic RO_2.

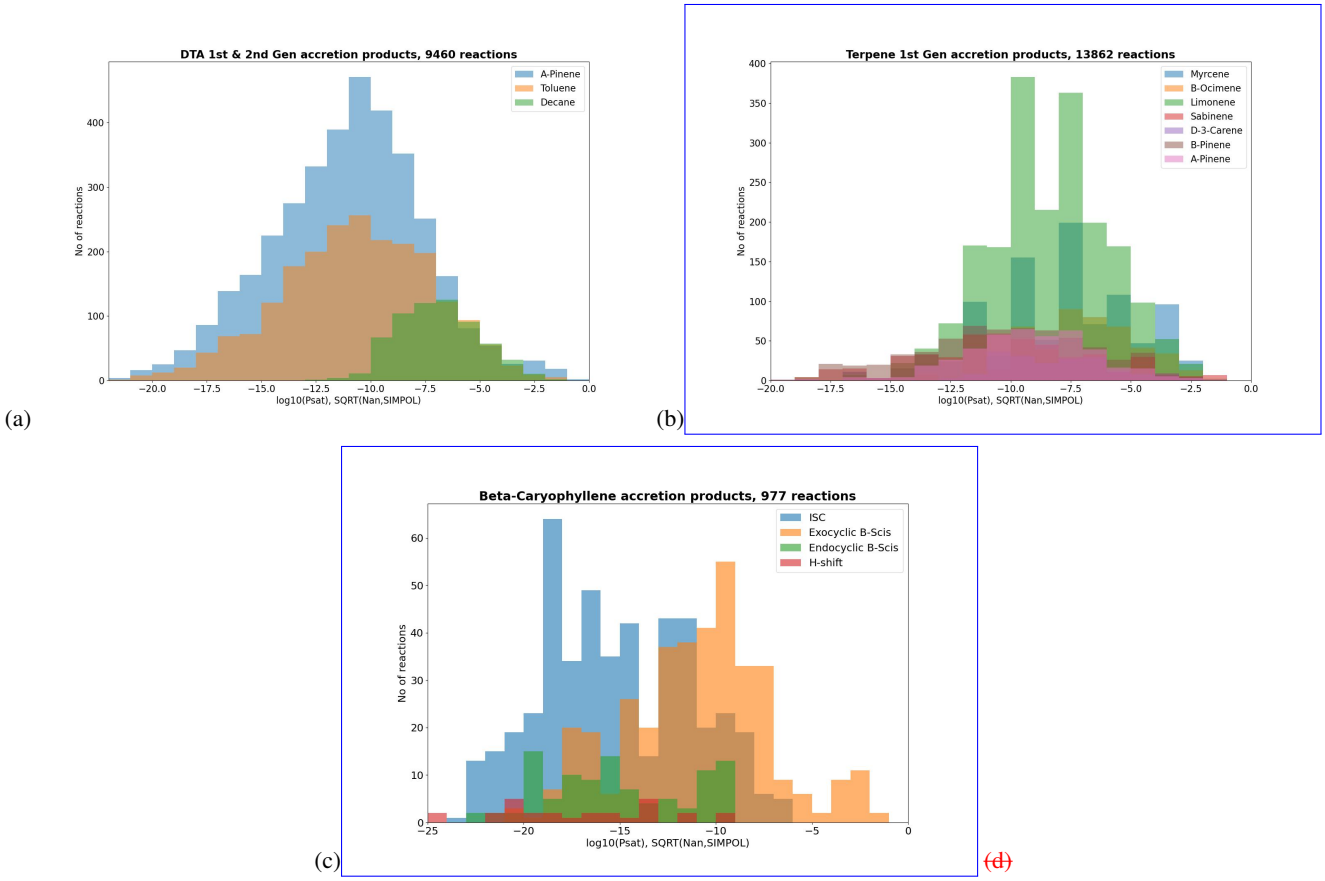

Figure 9. p_{Sat}-distributions of the early generation accretion products in each dataset categorized by precursor molecule. (a) ~~& (b)~~ Vapour pressure distribution in the DTA datset. (~~c~~b) ~~& (d)~~ Vapour pressure distribution in the Terpene dataset. ~~(b) & (d) are scaled by the product yields.~~

Figure 9 shows the early generation accretion products from the DTA and Terpene datasets categorized by precursor molecule, including only $RO_2 + RO_2$ pairs where both radicals are produced by the same precursor molecule. From the DTA

data we see rather unsurprisingly that α-pinene and Toluene are large sources of low volatility accretion products whereas n-Decane is not. In the Terpene results, we see that the lowest volatility bins ($p_{Sat} < 10^{-13}$ atm) are dominated by β-pinene and Sabinene, for less obvious reasons. Out of the 132 β-pinene derived 1st generation accretion products in these volatility bins, over half (68) were endocyclic β-scission channels. In all of these channels, the radical undergoing the decomposition is one of seven individual endocyclic RO combined with different pairs in the ^{3}(RO...OR) complex. Recognizable from these seven were three OH and ONO_2 addition derived radicals each: One with both rings intact and two with only the 4-ring intact. The seventh endocyclic RO is the VHP dissociation product of the C_9-Criegee Intermediate from β-pinene Ozonolysis. That these seven (out of 52 non-filtered 1st Gen RO_2 radicals) dominate the low-volatility accretion products is another example of the key role endocyclic β-scissions play in low volatility accretion product formation. For Sabinene, another interesting trend emerges: Only 40 out of the 100 $p_{Sat} < 10^{-13}$ atm accretion products are endocyclic β-scission products. 46 are ISC products, and 10 are H-shift products. Upon closer examination all four of the radicals undergoing the H-shift are primary RO in which Sabinene's 5-Carbon ring has already been broken. In the H-shift classification of Vereecken and Peeters (2010) these reactions are either secondary α-OH or tertiary β-exo-oxo shifts. None of these are major products, as the SAR never predicts H-shift rates above 10^8 s^{-1}, but these are nevertheless good examples of systems where the unimolecular H-shifts could be a competitive route to accretion product formation.

Another point worthy of discussion is the detail raised in Sect. 3.2 that Isoprene-derived RO_2 (Iso-RO_2) typically have high $RO_2 + RO_2$ reaction rates. This implies that cross reactions between Iso-RO_2 with the larger but less abundant monoterpene-derived RO_2 (Mono-RO_2) might be atmopherically significant. In Fig. 10 we see that the p_{Sat} values of these Iso-RO_2 + Mono-RO_2 products are not quite as low as those of Mono-RO_2 + Mono-RO_2, but a significant amount of them stretches below the 10^{-13} atm threshold nevertheless. We should also note that as our filtering method is based on relative product yields rather than product concentrations, we are likely underestimating the atmospheric occurrence of Iso-RO_2 + Mono-RO_2 pairs relative to Mono-RO_2 + Mono-RO_2 pairs, as global Isoprene emissions outnumber total monoterpene emissions threefold in terms of concentration according to Sindelarova et al. (2014) (sixfold in terms of mass in the original source), which roughly estimated means an on average 20-fold higher formation rate relative to the individual monoterpenes in the dataset. We thus suspect that Iso-RO_2 + Mono-RO_2 reactions are an atmospherically significant but understudied pathway to formation of $p_{Sat} < 10^{-9}$ atm contributing to aerosol particle growth, despite being experimentally less important than Mono-RO_2 + Mono-RO_2 for new particle formation according to Dada et al. (2023).

~~How do the~~ The results for β-caryophyllene ~~compare to the monoterpenes? In the end, not considerably. Figure ??c and f reproduce largely the same trends as Figure ??and d~~are comparable to those of monoterpenes, as seen in Figure 9c. However, we do see that the vapour pressure gap between the RO-fragmenting exocyclic β-scissions and the non-fragmenting endocyclic β-scission, H-shift and ISC products is even wider, a fact which is largely explained by the closed-shell products of the exocyclic β-scissions also being larger. What this tells us is that formation of ELVOCs from sesquiterpenes likely isn't qualitatively different from ELVOC formation from monoterpenes. Even with larger molecular sizes the ELVOC formation is

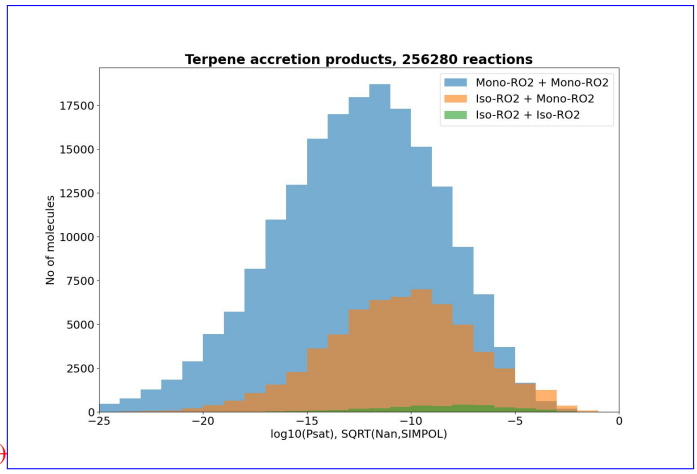

~~(a)(b)~~

Figure 10. p_{Sat}-distributions of the accretion products in the Terpene dataset categorized by type of RO_2 pair. ~~(b) is weighted by the product yield. MetC(O)O$_2$~~$CH_3C(O)O_2$-including pairs were separated from the rest due to their abundance, relatively high volatilities and due to ~~MetC(O)O$_2$~~ $CH_3C(O)O_2$ being formed from all precursors in the dataset.

probably still dominated by the handful of reaction channels that produce the fastest oxidation without too much fragmentation.

One interesting detail to consider is to which extent the use of SAR reaction rates and lack of RO_2 autoxidation misrepresents these trends. For the former, a recent computational study of β-scission rates in NO_3-derived monoterpene (Draper et al., 2024) RO provides an interesting point of comparison. For β-pinene in particular the computational ring-opening activation energies are considerably higher than in the SAR, partially due to stereoelectronic effects arising from the orientation of the exocyclic ONO_2 group and partially due to steric repulsion from the 4-carbon ring preventing the scission of the C-C bond connected to it. In terms of reaction rates it seems that none of the SAR-predicted competitive ($k_\beta > 10^8$ s^{-1}) endocyclic β-scissions of Limonene, β-pinene and Δ-3-carene are competitive anymore once one accounts for these new stereochemical effects. This underlines the limitations of the SAR models when dealing with especially complex molecules. On the impact of the missing autoxidation reactions, ~~an interesting example of this occurs when we~~ the importance of endocyclic RO_2 makes it especially notable that GECKO-A lacks most unimolecular RO_2 ring closure reactions, which adds competitive routes for forming endocyclic RO_2. The only such reaction included in the current version is the bicyclic RO_2 formation known from OH oxidation of aromatics (First reaction in Table 14 of Jenkin et al. (2019)). However, the work of Vereecken et al. (2021) shows that these reactions produces both endocyclic and exocyclic RO_2, of which the latter channel is more competitive in most cases. Nevertheless, the net increase of ring structures likely leads to formation of endocyclic RO_2 in the next generation with some probability. We might also compare our emphasis on endocyclic RO_2 formation on the established consensus on monoterpene oxidation. According to Lee et al. (2023) it is the *exocyclic* RO_2 formed after opening of the 4-carbon ring in α- and β-pinene that contributes the most to formation of low-volatility organics, at least among the OH-oxidation products.

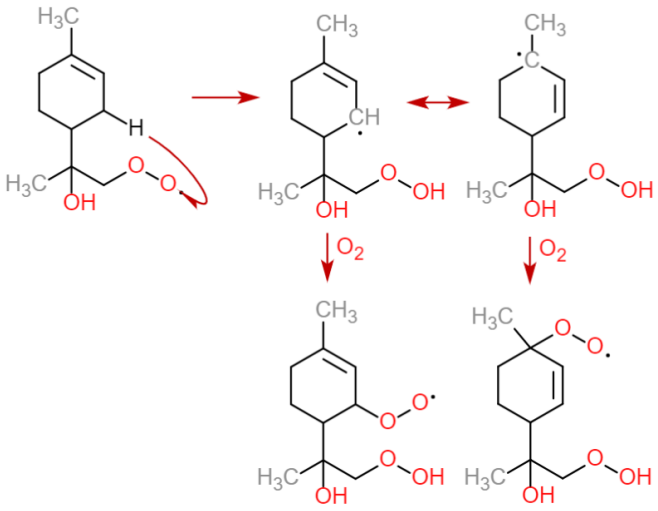

Figure 11. An autoxidation scheme for α-pinene derived endocyclic RO_2 with rapid RO β-scission rates, adapted from Møller et al. (2020).

While this may seems to be in conflict with our findings at first glance, we note that this contribution is due to a rapid H-shift reaction which leads to the formation of a (delocalized) endocyclic alkyl radical that may form two RO_2. (Fig 11) (Møller et al., 2020) Furthermore, applying the SAR to the corresponding RO leads to an endocyclic β-scission rate of $2 \cdot 10^{10}$ s^{-1} in both cases. In other words, the formation of low-volatility organics from this reaction channel is also likely driven by in-complex endocyclic β-scissions, and the lack of RO_2 autoxidation in GECKO-A only means that we are missing some of the reactions forming the most oxidized endocyclic RO_2.

3.5 Atmospheric Concentrations

The steady-state equations resulted in a total RO_2 concentration of $3.70 \cdot 10^9$ molecule cm^{-3} at daytime and $1.26 \cdot 10^9$ molecule cm^{-3} at nighttime. The daytime HO_2 concentration was $6.7 \cdot 10^8$ molecule cm^{-3}, which means that our $\frac{RO_2}{[HO_2]}$ ratio is within the Kenagy et al. (2024) probability distribution we were aiming for. In Table 5, we see how the high RO_2 concentration translated to reactivities (Eq. 9a, i.e. the freaction of RO_2 reacting with other RO_2) for different kinds of RO_2. CH_3O_2 reactivities are also presented, as all of these reactions were neglected in the GECKO-AP code. In Eq. 9a α is the Jenkin rate class of the RO_2 the quantity is calcualted for. Once again we see a strong contrast between the classes of RO_2 with fast $RO_2 + RO_2$ rates and classes with slow $RO_2 + RO_2$ rates in the Jenkin et al. (2019) parametrization. RC(O)O_2 and β-substituted primary RO_2 react primarily with other RO_2 at sufficiently low-NO_x conditions, whereas secondary and especially tertiary RO_2 react primarily with inorganic radicals. We also see greatly elevated RO_2 reactivities at night due to lower concentrations of RO_2 scavengers NO, HO_2, and (to a lesser extent) OH. This suggests that accretion product formation from $RO_2 + RO_2$ reactions might be more important at nighttime, all else being equal. The important caveat here is that all else *isn't* equal in real diurnal cycles, in part due to generally lower RO_2 production with lower biogenic emission rates. Box modelling studies will have to be performed

to determine which effect is dominant. Another interesting detail is that CH_3O_2 was only responsible for a small fraction of the RO_2 reactivity, despite CH_3O_2 being known as the major atmospheric peroxy radical (Wayne, 2000). This may be explained by the fact that CH_3O_2 has no primary source besides $CH_4 + OH$, for which the rate coefficient is over four orders of magnitude slower than of Isoprene + OH (Seinfeld and Pandis, 2016), which makes Isoprene oxidation the far bigger source of RO_2 in these relative concentrations. This is a very promising result for the importance of the accretion product formation studied in this work, but it should be noted that the Isoprene concentrations used here are only representative of environments close to emission sources, due to the short atmospheric lifetime (Wennberg et al., 2018). CH_3O_2 is thus more likely to dominate $RO_2 + RO_2$ reactions in environments far away from both alkene emission sources. These

$$\mathrm{RO_2\ R.}(\alpha) \equiv \frac{\sum_\beta^9 k_{\mathrm{RO_2RO_2},\alpha+\beta}[\mathrm{RO_{2\beta}}]}{\sum_j^5 k_{\mathrm{RO_2Ox}_j}[\mathrm{Ox}_j] + \sum_\beta^9 k_{\mathrm{RO_2RO_2},\alpha+\beta}[\mathrm{RO_{2\beta}}]} \tag{9a}$$

$$\mathrm{CH_3O_2\ R.}(\alpha) \equiv \frac{k_{\mathrm{RO_2RO_2},\alpha+6}[\mathrm{CH_3O_2}]}{\sum_j^5 k_{\mathrm{RO_2Ox}_j}[\mathrm{Ox}_j] + \sum_\beta^9 k_{\mathrm{RO_2RO_2},\alpha+\beta}[\mathrm{RO_{2\beta}}]} \tag{9b}$$

Type	No	c (Day)	c (Night)	RO_2 R. (Day)	RO_2 R. (Night)	CH_3O_2 R. (Day)	CH_3O_2 R. (Night)
$RC(O)O_2$	24	$2.23{\cdot}10^7$	$4.60{\cdot}10^6$	61.30 %	94.40 %	2.88 %	2.26 %
Prim-RO_2	50	$1.39{\cdot}10^9$	$2.09{\cdot}10^7$	47.55 %	88.98 %	1.02 %	1.93 %
Sec-RO_2	62	$8.90{\cdot}10^8$	$6.78{\cdot}10^7$	21.49 %	67.52 %	0.45 %	1.40 %
Tert-RO_2	54	$1.40{\cdot}10^9$	$1.17{\cdot}10^9$	3.35 %	16.81 %	0.06 %	0.43 %

Table 5. Concentrations as well as RO_2 and CH_3O_2 reactivities by RO_2 type in the steady-state solution.

The estimated RO_2 concentrations can further be used to estimate accretion product formation rates for the Isoprene-derived products in the Terpene dataset, through $k_{\mathrm{RO_2RO_2},\alpha\beta}[\alpha][\beta] \cdot \frac{k_r}{k_{ISC}+\sum_i^{n_\alpha} k_i + \sum_j^{n_\beta} k_j}$, by combining the concentrations with Eq. 4 and 6. This results in a total daytime formation rate of $3.838 \cdot 10^6$ molecule cm^{-3} s^{-1} and nighttime formation rate of $1.240 \cdot 10^4$ molecule cm^{-3} s^{-1} for ROOR-type accretion products, whereas for our RO decomposition derived ether and ester type accretion products the daytime formation rate is $9.472 \cdot 10^6$ molecule cm^{-3} s^{-1} and nighttime rate is $1.958 \cdot 10^4$ molecule cm^{-3} s^{-1}. Since the latter reactions include an additional fragmentation step it is worth noting that a majority of the formed ethers and esters ($5.372 \cdot 10^6$ molecule cm^{-3} s^{-1} and $1.783 \cdot 10^4$ molecule cm^{-3} s^{-1} at day and night, respectively) have more than Isoprene's five carbon atoms. We expect the observed difference between daytime and nighttime rates to be mostly Isoprene-specific, due to the exceptionally fast OH addition rate and due to the faster recombination rates of the most important daytime Isoprene-RO_2. The fact that Jenkin's SAR for RO_2 self-reactions lacks activation parameters for nitrate groups (Jenkin et al., 2019) may also play a role in underestimation of important nighttime radicals. The latter daytime value is almost 20 % of the product formation rate from $RO_2 + HO_2$, assuming an upper-limit rate coefficient of $2 \cdot 10^{-11}$ cm^3 molecule^{-1} s^{-1} and the daytime concentrations mentioned above, suggesting that these ether and ester accretion products are an important part

of RO_2 chemistry in low NO_x, high VOC environments. More analysis of the results are found in Section S8 of the Supplement.

4 Conclusions

In our previous work (Peräkylä et al., 2023) we observed that rapid decomposition of alkoxy radicals in the ^{3}(RO…OR) intermediates of peroxy radical recombination reactions may form ether and ester accretion products in addition to the already known peroxides. In this work we looked at a wider range of rapid alkoxy radical decomposition reactions to explore the full atmospheric implications of this new observed channel. While our quantitative data rests on a mountain of assumptions concerning the rates of the competing channels, we can already discern several qualitatively reliable trends:

- Our previously observed in-complex alkoxy radical decomposition was a β-scission reaction. By systematically looking at all the known reactions of free alkoxy radicals, we have concluded that the β-scission is often the most important in-complex RO decomposition channel.

- Furthermore, the most competitive β-scission reactions are endocyclic β-scissions, which produce products of the same mass as the known ROOR peroxide product. These have likely been produced in many previous experiments, but eluded identification due to the use of mass spectrometric detection methods.

- The products of exocyclic β-scission reactions typically have higher vapour pressures than the corresponding ROOR, which is to be expected as they are smaller molecules. However, as these are ethers or esters rather than peroxides, they will be more stable towards both photochemical and thermal decomposition, as well as fragmenting oxidation, and thus more likely to contribute to SOA formation and growth.

- Unimolecular alkoxy radical H-shift reactions are rarely competitive with the β-scissions, but their products typically have lower vapour pressures than any other peroxy radical recombination products. These reactions might be very important for SOA formation from a small specific subset of peroxy radical recombinations.

- Acyl peroxy radicals are especially interesting for accretion product formation from peroxy radial recombination due to their ability to readily react with large tert-RO_2 with otherwise slow $RO_2 + RO_2$ rates.

- It has recently been postulated that the branching ratio of accretion product forming channels of peroxy radical recombination will progressively increase with RO_2 size and oxidation state. (Hasan, 2023) This may not always be the case thanks to alkoxy decomposition reactions where the products are a closed-shell organic molecule and a small inorganic radical. These reactions grow increasingly likely as the number of hydroperoxide, nitrate and nitro groups in the reactant peroxy radicals increase.

~~Data Availability~~

Data Availability The datasets generated by the code ~~will be~~ are available in a Zenodo repository (https://zenodo.org/records/13253425) once the article is accepted for publication. This data includes labelled Peroxy radical lists, Peroxy radical pair lists, in-complex alkoxy radical reaction lists, and accretion product lists with various levels of filtering. The ORCA output files of the computational results presented in Sect. S3 of the Supplement and the calculated steady-state concentations for the Isoprene-derived radicals and accretion products are also included here.

~

~~Supplement~~

Supplement The supplement related to this article is available online at (DOI).

~

~~Author Contibutions~~

Author Contributions LF wrote the GECKO-AP code, performed the data analysis on the generated datasets, and drafted the manuscript. MC, RV and BA provided help and consultation on usage of the GECKO-A code, and advice on how to filter, analyse and represent the data. The original idea was envisioned by TK. The manuscript was reviewed and revised by all authors.

~

~~Competing Interests~~

Competing Interests The authors declare that they have no conflict of interest.

~

~~Acknowledgements~~

Acknowledgements This work was supported by the Academy of Finland through the Virtual Laboratory for Molecular Level Atmospheric Transformations Centre of Excellence (VILMA) as well as the Jane ja Aatos Erkon Säätiö Foundation. Computational resources for the quantum chemical scans were provided by the Finnish Centre for Scientific Computing (CSC). L.F. personally thanks Matti Rissanen for useful discussions on the reactivity of acyl peroxy radicals, Siddharth Iyer on toluene oxidation, Vili-Taneli Salo on recent computational findings of tetroxide decomposition, Rashid Valiev for trends and uncertainties on ^{3}(RO…OR) ISC rates, and Emelda Ahongshangbam for ROOOH reactions. William Carter and an anonymous

referee are gratefully acknowledged for review and discussion that helped to improve the article, and Thomas Berkemeier for editing it.

References

Anglada, J. M. and Solé, A.: Tropospheric oxidation of methyl hydrotrioxide (CH_3OOOH) by hydroxyl radical, Physical Chemistry Chemical Physics, 20, 27 406–27 417, 2018.

Assaf, E., Schoemaecker, C., Vereecken, L., and Fittschen, C.: Experimental and theoretical investigation of the reaction of RO2 radicals with OH radicals: Dependence of the HO2 yield on the size of the alkyl group, International journal of chemical kinetics, 50, 670–680, 2018.

Aumont, B., Szopa, S., and Madronich, S.: Modelling the evolution of organic carbon during its gas-phase tropospheric oxidation: development of an explicit model based on a self generating approach, Atmospheric Chemistry and Physics, 5, 2497–2517, 2005.

Berndt, T., Richters, S., Kaethner, R., Voigtländer, J., Stratmann, F., Sipilä, M., Kulmala, M., and Herrmann, H.: Gas-phase ozonolysis of cycloalkenes: formation of highly oxidized RO_2 radicals and their reactions with NO, NO_2, SO_2, and other RO_2 radicals, The Journal of Physical Chemistry A, 119, 10 336–10 348, 2015.

Berndt, T., Chen, J., Kjærgaard, E. R., Møller, K. H., Tilgner, A., Hoffmann, E. H., Herrmann, H., Crounse, J. D., Wennberg, P. O., and Kjaergaard, H. G.: Hydrotrioxide (ROOOH) formation in the atmosphere, Science, 376, 979–982, 2022.

Besel, V., Todorović, M., Kurtén, T., Rinke, P., and Vehkamäki, H.: Atomic structures, conformers and thermodynamic properties of 32k atmospheric molecules, Scientific Data, 10, 450, 2023.

Bey, I., Aumont, B., and Toupance, G.: The nighttime production of OH radicals in the continental troposphere, Geophysical research letters, 24, 1067–1070, 1997.

Bianchi, F., Kurtén, T., Riva, M., Mohr, C., Rissanen, M. P., Roldin, P., Berndt, T., Crounse, J. D., Wennberg, P. O., Mentel, T. F., et al.: Highly oxygenated organic molecules (HOM) from gas-phase autoxidation involving peroxy radicals: A key contributor to atmospheric aerosol, Chemical reviews, 119, 3472–3509, 2019.

Compernolle, S., Ceulemans, K., and Müller, J.-F.: Vapor pressure estimation methods applied to secondary organic aerosol constituents from α-pinene oxidation: an intercomparison study, Atmospheric Chemistry and Physics, 10, 6271–6282, 2010.

Dada, L., Stolzenburg, D., Simon, M., Fischer, L., Heinritzi, M., Wang, M., Xiao, M., Vogel, A. L., Ahonen, L., Amorim, A., et al.: Role of sesquiterpenes in biogenic new particle formation, Science Advances, 9, eadi5297, 2023.

Draper, D., Almeida, T. G., Iyer, S., Smith, J. N., Kurtén, T., and Myllys, N.: Unpacking the diversity of monoterpene oxidation pathways via nitrooxy–alkyl radical ring-opening reactions and nitrooxy–alkoxyl radical bond scissions, Journal of Aerosol Science, 179, 106 379, 2024.

Ehn, M., Thornton, J. A., Kleist, E., Sipilä, M., Junninen, H., Pullinen, I., Springer, M., Rubach, F., Tillmann, R., Lee, B., et al.: A large source of low-volatility secondary organic aerosol, Nature, 506, 476–479, 2014.

Franzon, L.: Simple Physical Model for the Estimation of Irreversible Dissociation Rates for Bimolecular Complexes, The Journal of Physical Chemistry A, 127, 5956–5966, 2023.

Hasan, G.: Computational Studies of Reaction Channels for ^{3}(RO…OR) Intermediates formed in Peroxy Self and Cross-Reactions, Ph.D. thesis, University of Helsinki, 2023.

Hasan, G., Salo, V.-T., Golin Almeida, T., Valiev, R. R., and Kurtén, T.: Computational Investigation of Substituent Effects on the Alcohol+ Carbonyl Channel of Peroxy Radical Self-and Cross-Reactions, The Journal of Physical Chemistry A, 127, 1686–1696, 2023.

Ingold, K. U.: Peroxy radicals, Accounts of Chemical Research, 2, 1–9, 1969.

Isaacman-VanWertz, G. and Aumont, B.: Impact of organic molecular structure on the estimation of atmospherically relevant physicochemical parameters, Atmospheric Chemistry and Physics, 21, 6541–6563, 2021.

Jenkin, M. E., Valorso, R., Aumont, B., Rickard, A. R., and Wallington, T. J.: Estimation of rate coefficients and branching ratios for gas-phase reactions of OH with aliphatic organic compounds for use in automated mechanism construction, Atmospheric Chemistry and Physics, 18, 9297–9328, 2018a.

Jenkin, M. E., Valorso, R., Aumont, B., Rickard, A. R., and Wallington, T. J.: Estimation of rate coefficients and branching ratios for gas-phase reactions of OH with aromatic organic compounds for use in automated mechanism construction, Atmospheric Chemistry and Physics, 18, 9329–9349, 2018b.

Jenkin, M. E., Valorso, R., Aumont, B., and Rickard, A. R.: Estimation of rate coefficients and branching ratios for reactions of organic peroxy radicals for use in automated mechanism construction, Atmospheric Chemistry and Physics, 19, 7691–7717, 2019.

Jenkin, M. E., Valorso, R., Aumont, B., Newland, M. J., and Rickard, A. R.: Estimation of rate coefficients for the reactions of O 3 with unsaturated organic compounds for use in automated mechanism construction, Atmospheric Chemistry and Physics, 20, 12 921–12 937, 2020.

Kanakidou, M., Seinfeld, J., Pandis, S., Barnes, I., Dentener, F. J., Facchini, M. C., Van Dingenen, R., Ervens, B., Nenes, A., Nielsen, C., et al.: Organic aerosol and global climate modelling: a review, Atmospheric Chemistry and Physics, 5, 1053–1123, 2005.

Kenagy, H., Heald, C., Tahsini, N., Goss, M., and Kroll, J.: Can we achieve atmospheric chemical environments in the laboratory? An integrated model-measurement approach to chamber SOA studies, In Review, 2024.

Kerdouci, J., Picquet-Varrault, B., and Doussin, J.-F.: Prediction of Rate Constants for Gas-Phase Reactions of Nitrate Radical with Organic Compounds: A New Structure–Activity Relationship, ChemPhysChem, 11, 3909–3920, 2010.

Kerdouci, J., Picquet-Varrault, B., and Doussin, J.-F.: Structure–activity relationship for the gas-phase reactions of NO3 radical with organic compounds: Update and extension to aldehydes, Atmospheric Environment, 84, 363–372, 2014.

Knap, H. C. and Jørgensen, S.: Rapid hydrogen shift reactions in acyl peroxy radicals, The Journal of Physical Chemistry A, 121, 1470–1479, 2017.

Kurtén, T., Tiusanen, K., Roldin, P., Rissanen, M., Luy, J.-N., Boy, M., Ehn, M., and Donahue, N.: α-Pinene autoxidation products may not have extremely low saturation vapor pressures despite high O: C ratios, The Journal of Physical Chemistry A, 120, 2569–2582, 2016.

Lee, B. H., Iyer, S., Kurtén, T., Varelas, J. G., Luo, J., Thomson, R. J., and Thornton, J. A.: Ring-opening yields and auto-oxidation rates of the resulting peroxy radicals from OH-oxidation of α-pinene and β-pinene, Environmental Science: Atmospheres, 3, 399–407, 2023.

Méreau, R., Rayez, M.-T., Rayez, J.-C., Caralp, F., and Lesclaux, R.: Theoretical study on the atmospheric fate of carbonyl radicals: kinetics of decomposition reactions, Physical Chemistry Chemical Physics, 3, 4712–4717, 2001.

Møller, K. H., Otkjær, R. V., Chen, J., and Kjaergaard, H. G.: Double bonds are key to fast unimolecular reactivity in first-generation monoterpene hydroxy peroxy radicals, The Journal of Physical Chemistry A, 124, 2885–2896, 2020.

Murphy, S. E., Crounse, J. D., Møller, K. H., Rezgui, S. P., Hafeman, N. J., Park, J., Kjaergaard, H. G., Stoltz, B. M., and Wennberg, P. O.: Accretion product formation in the self-reaction of ethene-derived hydroxy peroxy radicals, Environmental Science: Atmospheres, 3, 882–893, 2023.

Nannoolal, Y., Rarey, J., Ramjugernath, D., and Cordes, W.: Estimation of pure component properties: Part 1. Estimation of the normal boiling point of non-electrolyte organic compounds via group contributions and group interactions, Fluid Phase Equilibria, 226, 45–63, 2004.

Nannoolal, Y., Rarey, J., and Ramjugernath, D.: Estimation of pure component properties: Part 3. Estimation of the vapor pressure of non-electrolyte organic compounds via group contributions and group interactions, Fluid Phase Equilibria, 269, 117–133, 2008.

Neese, F.: Software update: The ORCA program system - Version 5.0, WIREs Computational Molecular Science, 12, https://doi.org/10.1002/wcms.1606, 2022.

Newland, M. J., Mouchel-Vallon, C., Valorso, R., Aumont, B., Vereecken, L., Jenkin, M. E., and Rickard, A. R.: Estimation of mechanistic parameters in the gas-phase reactions of ozone with alkenes for use in automated mechanism construction, Atmospheric Chemistry and Physics, 22, 6167–6195, 2022.

Novelli, A., Cho, C., Fuchs, H., Hofzumahaus, A., Rohrer, F., Tillmann, R., Kiendler-Scharr, A., Wahner, A., and Vereecken, L.: Experimental and theoretical study on the impact of a nitrate group on the chemistry of alkoxy radicals, Physical Chemistry Chemical Physics, 23, 5474–5495, 2021.

Orlando, J. J. and Tyndall, G. S.: Laboratory studies of organic peroxy radical chemistry: an overview with emphasis on recent issues of atmospheric significance, Chemical Society Reviews, 41, 6294–6317, 2012.

Orlando, J. J., Tyndall, G. S., and Wallington, T. J.: The atmospheric chemistry of alkoxy radicals, Chemical reviews, 103, 4657–4690, 2003.

Pankow, J. F. and Asher, W. E.: SIMPOL. 1: a simple group contribution method for predicting vapor pressures and enthalpies of vaporization of multifunctional organic compounds, Atmospheric Chemistry and Physics, 8, 2773–2796, 2008.

Peräkylä, O., Berndt, T., Franzon, L., Hasan, G., Meder, M., Valiev, R. R., Daub, C. D., Varelas, J. G., Geiger, F. M., Thomson, R. J., et al.: Large Gas-Phase Source of Esters and Other Accretion Products in the Atmosphere, Journal of the American Chemical Society, 145, 7780–7790, 2023.

Platz, J., Nielsen, O., Wallington, T., Ball, J., Hurley, M., Straccia, A., Schneider, W., and Sehested, J.: Atmospheric chemistry of the phenoxy radical, $C_6H_5O\cdot$: UV spectrum and kinetics of its reaction with NO, NO2, and O2, The Journal of Physical Chemistry A, 102, 7964–7974, 1998.

Rissanen, M. P., Kurtén, T., Sipilä, M., Thornton, J. A., Kangasluoma, J., Sarnela, N., Junninen, H., Jørgensen, S., Schallhart, S., Kajos, M. K., et al.: The formation of highly oxidized multifunctional products in the ozonolysis of cyclohexene, Journal of the American Chemical Society, 136, 15 596–15 606, 2014.

Russell, G. A.: Deuterium-isotope effects in the autoxidation of aralkyl hydrocarbons. mechanism of the interaction of peroxy radicals, Journal of the American Chemical Society, 79, 3871–3877, 1957.

Salo, V.-T., Chen, J., Runeberg, N., Kjaergaard, H. G., and Kurtén, T.: Multireference and Coupled-Cluster Study of Dimethyltetroxide (MeO4Me) Formation and Decomposition, The Journal of Physical Chemistry A, 2024.

Seinfeld, J. H. and Pandis, S. N.: Atmospheric chemistry and physics: from air pollution to climate change, John Wiley & Sons, 2016.

Sindelarova, K., Granier, C., Bouarar, I., Guenther, A., Tilmes, S., Stavrakou, T., Müller, J.-F., Kuhn, U., Stefani, P., and Knorr, W.: Global data set of biogenic VOC emissions calculated by the MEGAN model over the last 30 years, Atmospheric Chemistry and Physics, 14, 9317–9341, 2014.

Topping, D.: UManSysProp Multiphase system online property prediction, http://http://umansysprop.seaes.manchester.ac.uk.

Valorso, R., Aumont, B., Camredon, M., Raventos-Duran, T., Mouchel-Vallon, C., Ng, N., Seinfeld, J. H., Lee-Taylor, J., and Madronich, S.: Explicit modelling of SOA formation from α-pinene photooxidation: sensitivity to vapour pressure estimation, Atmospheric Chemistry and Physics, 11, 6895–6910, 2011.

Vereecken, L.: Computational study of the stability of α-nitroxy-substituted alkyl radicals, Chemical Physics Letters, 466, 127–130, 2008.

Vereecken, L. and Nozière, B.: H migration in peroxy radicals under atmospheric conditions, Atmospheric chemistry and physics, 20, 7429–7458, 2020.

Vereecken, L. and Peeters, J.: Decomposition of substituted alkoxy radicals—part I: a generalized structure–activity relationship for reaction barrier heights, Physical Chemistry Chemical Physics, 11, 9062–9074, 2009.

Vereecken, L. and Peeters, J.: A structure–activity relationship for the rate coefficient of H-migration in substituted alkoxy radicals, Physical Chemistry Chemical Physics, 12, 12 608–12 620, 2010.

Vereecken, L., Nguyen, T. L., Hermans, I., and Peeters, J.: Computational study of the stability of α-hydroperoxyl-or α-alkylperoxyl substituted alkyl radicals, Chemical physics letters, 393, 432–436, 2004.

Vereecken, L., Vu, G., Wahner, A., Kiendler-Scharr, A., and Nguyen, H.: A structure activity relationship for ring closure reactions in unsaturated alkylperoxy radicals, Physical Chemistry Chemical Physics, 23, 16 564–16 576, 2021.

Wayne, R. P.: Chemistry of Atmospheres, 3rd Edition, Oxford University Press, Oxford, England, 2000.

Wennberg, P. O., Bates, K. H., Crounse, J. D., Dodson, L. G., McVay, R. C., Mertens, L. A., Nguyen, T. B., Praske, E., Schwantes, R. H., Smarte, M. D., et al.: Gas-phase reactions of isoprene and its major oxidation products, Chemical reviews, 118, 3337–3390, 2018.